Spectroscopic and Functional Characterization of Nitrophorin 7 from the Blood-Feeding Insect *Rhodnius prolixus* Reveals an Important Role of Its Isoform-Specific N-Terminus for Proper Protein Function†

Markus Knipp,*,‡ Fei Yang, Robert E. Berry, Hongjun Zhang, Maxim N. Shokhirev, and F. Ann Walker

Department of Chemistry, The University of Arizona, 1306 East University Boulevard, Tucson, Arizona 85721-0041

Received July 26, 2007; Revised Manuscript Received September 6, 2007

ABSTRACT: Nitrophorins (NPs) are a class of NO-transporting and histamine-sequestering heme *b* proteins that occur in the saliva of the bloodsucking insect *Rhodnius prolixus*. A detailed study of the newly described member, NP7, is presented herein. NO association constants for NP7 [K_{eq}^{III}(NO)] reveal a drastic change when the pH is varied from 5.5 (reflecting the insect's saliva) to slightly above plasma pH (7.5) ($>10^9$ $M^{-1} \rightarrow 4.0 \times 10^6$ M^{-1}); thus, the protein promotes the storage of NO in the insect's saliva and its release inside the victim's tissues. In contrast to the other nitrophorins, NP1−4, histamine sequestering cannot be accomplished in vivo due to the low binding constant [K_{eq}^{III}(histamine)] of 10^5 M^{-1} compared to the histamine concentration of $1-10 \times 10^{-9}$ M in the blood. A major part of this study deals with the N-terminus, ^{1}Leu-Pro-Gly-Glu-Cys^5 of NP7, which is not found in NP1−4. Since NP7 has not been isolated from the insects but was recognized in a cDNA library instead, the N-terminal site of signal peptidase cleavage upon protein secretion was predicted by the program SIGNALP [Andersen, J. F., Gudderra, N. P., Francischetti, I. M. B., Valenzuela, J. G., and Ribeiro, J. M. C. (2004) *Biochemistry 43*, 6987−6994]. In marked contrast to wild-type NP7, NP7(Δ1−3) exhibits a very high NO affinity at pH 7.5 [K_{eq}^{III}(NO) $\approx$ 10^9 M^{-1}], suggesting that the release of NO in the plasma cannot efficiently be accomplished by the truncated form. Comparison of the reduction potentials of both constructs by spectroelectrochemistry revealed an average increase of +85 mV for various distal ligands bound to the heme iron when the ^{1}Leu-Pro-Gly^3 peptide was removed. However, ^{1}H NMR and EPR spectroscopy show that the electronic properties of the Fe^{III} cofactor are similar in both wild-type NP7 and NP7(Δ1−3). Further, thermal denaturation that revealed a higher stability of wild-type NP7 compared to NP7(Δ1−3), in combination with a homology model based on the NP2 crystal structure (rmsd = 0.39 Å), suggests that interaction of the ^{1}Leu-Pro-Gly^3 peptide with the A−B and/or G−H loops is key for proper protein function.

The "kissing bug" *Rhodnius prolixus* is an important vector of Chagas' disease, one of the world's most widespread lethal diseases transmitted by bloodsucking insects (*1*, *2*). The insect spreads the protozoan *Trypanosoma cruzi*, a parasite living in the insect's gut, through defecation at the site of the bite (*3*). A death toll of 15 000 persons per year from this disease was reported in 2004 according to the World Health Organization,[1] and there are probably many more victims for whom the disease was not diagnosed. The overwhelming majority of infected persons (16−18 million people) live in South and Central America (*2*), but the disease has, however, migrated as far north as the southern United States, including California, Arizona, and Texas, which puts many more people at risk of infection (*4*, *5*). This situation led to the careful investigation of the biology and physiological processes involved in the vector ↔ host interaction.

The nitrophorins (NPs)[2] represent a group of NO-carrying heme proteins found in the saliva of *R. prolixus* (*6*), which in its adult phase expresses at least four nitrophorins, designated NP1−4 in order of their decreasing abundance in the saliva of adult insects (*1*, *7*). Before *R. prolixus* reaches the adult phase, it develops through five instar nymphal stages (*3*). Two additional nitrophorins, designated NP5 and NP6, have been detected mainly in the five instar nymphal stages of insect development (*8*). Nitrophorins are expressed in the endothelial cells of the salivary gland where an N-terminal signal sequence leads them to be secreted before it is truncated. After the salivary glands are loaded with

† This work was financially supported by the Swiss National Science Foundation (SNF), Grant PA00A--109035 (to M.K.), and by the National Institutes of Health (NIH), Grant HL54826 (to F.A.W.).

* To whom correspondence should be addressed. Telephone: +49 (0)208 306 4. Fax: +49 (0)208 306 3951. E-mail: mknipp@mpi-muelheim.mpg.de.

‡ Present address: Max Planck Institute for Bioinorganic Chemistry, Stiftstrasse 34-36, D-45470 Mülheim an der Ruhr, Germany.

[1] World Health Report 2004, http://www.who.int/tdr/diseases/default.htm.

[2] Abbreviations: DEA/NO, sodium (*Z*)-1-(*N*,*N*-diethylamino)diazen-1-ium 1,2-diolate; Hm, histamine; HMM, hidden Markov model; HSA, human serum albumin; ImH, imidazole; L, distal ligand on heme iron; MALDI, matrix-assisted laser desorption ionization; Mb, myoglobin; MOPS, 3-(*N*-morpholino)propanesulfonic acid; NN, neuronal network; NOS, nitric oxide synthase; NP, nitrophorin; pH*, pH in D_2O solutions uncorrected for the deuterium effect; PS, L-α-phosphatidyl-L-serine; sGC, soluble guanylate cyclase; SHE, standard hydrogen electrode; SNAP, *S*-nitroso-*N*-acetyl-D,L-penicillamine; TOF, time-of-flight; *wt*, wild type.

10.1021/bi7014986 CCC: $37.00
Published on Web 10/24/2007

nitrophorins, a nitric oxide synthase (NOS) in the endothelium is turned on and charges the nitrophorin heme *b* cofactor with NO (*9*−*11*). The low pH of the saliva (5−6) (*12*) stabilizes the Fe^{III}−NO complex (*13*). In contrast to other heme proteins, e.g., myoglobin (Mb), which are reduced by excess NO (*14*), nitrophorins stabilize the Fe^{III} state by having a number of carboxylates near the heme pocket (R. E. Berry, M. N. Shokhirev, A. Y. W. Ho, H. Zhang, and F. A. Walker, manuscript to be submitted) and a ruffled heme geometry which is induced mainly by two Leu side chains that point toward the distal side of the heme (*15*). This way, the reduction potential is established at, for example, −303 mV versus SHE at pH 7.5 for NP1 compared to ∼0 mV versus SHE for Mb (*16*). This is important for nitrophorin function because Fe^{II}−NO association constants are too large to allow sufficient NO release [$K_{eq}^{II}(NO) = 10^{13}-10^{14}$ M^{-1}] (*17*).

When the bloodsucker feeds on a victim, the insect pumps the saliva in boluses with a mean frequency of 0.51 Hz into the victim through the saliva canal while pumping out the victim's blood through the feeding canal at the same time (*2*, *12*). The drastic pH change to that of the blood plasma (∼7.4) induces a conformational change in the nitrophorin structure that decreases the NO affinity 1−2 orders of magnitude and concomitantly leads, together with the large dilution (estimated to be a factor of 100 in the tissues, but would be higher in the blood stream), to the release of NO.

NO acts as a vasodilator and a platelet aggregation inhibitor, both of which benefit the insect during feeding. In addition, the imidazole group of histamine (Hm), which is released from mast cells at the site of the bite as an immune stimulus (*18*), binds to the open coordination site of the iron; thus, *R. prolixus* nitrophorins act as histamine traps and contribute to the immune response suppression (*19*) during the time of feeding (10−30 min) (*2*, *3*).

NP1−4 have been investigated by a number of spectroscopic techniques (*15*, *16*, *20*−*27*), spectroelectrochemistry (*1*, *15*, *16*, *21*, *28*), and stopped-flow kinetics (*28*−*30*), and the solid-state structures of several ligand complexes of NP1 (*16*, *31*), NP2 (*32*; A. Weichsel, R. E. Berry, F. A. Walker, and W. R. Montfort, manuscript to be submitted), and NP4 (*30*, *33*−*35*) have been determined by X-ray crystallography. The structures are unique for heme proteins, in that the heme is located at the open end of a β-barrel (*36*), rather than in the more commonly observed largely α-helical globin or four-helix bundle folds. The ferriheme prosthetic group is bound to the protein via a His ligand, leaving the sixth coordination site available to bind NO or other ligands.

Another nitrophorin (NP7) has recently been found in a cDNA library generated from salivary glands of V^{th} instar nymphs (*37*, *38*), but the protein has never been isolated from the insects. Of all the *R. prolixus* NPs discovered, NP7 is especially interesting since it was found to bind to L-α-phosphatidyl-L-serine (PS) containing phospholipid membranes which NP1−4 do not do (*38*, *39*). In platelets and mast cells, the loss of membrane asymmetry, which leads to the display of PS on the outer surface, is rapid and tightly coupled with other activation events, making it a highly reliable indicator of hemostatic activity and degranulation. NP1−4 would, therefore, remain in solution, diffusing away from the feeding site while releasing NO over a larger area. Recognition of PS exposure by proteins is important in biological processes such as the assembly of coagulation complexes and the clearance of apoptotic cells by macrophages (*40*, *41*). Thus, NP7 recognizes PS-bearing membrane surfaces as an indicator of activation and uses this as a means of targeting the surfaces of activated platelets and degranulating mast cells. Once bound on an activated platelet, NP7 can release NO to inhibit platelet aggregation and act as an anticoagulant by blocking coagulation factor binding sites.

NO is highly reactive in a biological environment [$t_{1/2} \approx$ 100 ms in blood (*42*)] but is protected from oxidation when bound to NPs (*16*). Targeted delivery to activated surfaces at the point of feeding may enhance the activity of NP7 as a platelet aggregation inhibitor by delivering NO in a protected form to its site of action and preventing its removal from the feeding area by diffusion and blood flow.

Although NP1−4 have been extensively studied and are structurally well-characterized, it remains a matter of debate why *R. prolixus* uses a whole bundle of NPs instead of just one, as seems to be the case with *Cimex lectularius* (the bedbug) (*43*). In addition, it remains unclear why the six life stages of *R. prolixus* (five instar nymphs and the adult stage) use different expression patterns of NPs (*8*). To answer these questions, comparative investigations of all NPs are required. Furthermore, we want to understand the properties of NP7 as a unique NO delivery system to cell surfaces, and thus, the characterization of NP7 properties in comparison to those of the established NP1−4 is a necessary step.

EXPERIMENTAL PROCEDURES

Materials. NP1 and NP2 were expressed and purified as previously described (*44*). *S*-Nitroso-*N*-acetyl-D,L-penicillamine (SNAP) was bought from World Precision Instruments. NO gas (98.5%), methyl viologen dichloride hydrate, anthraquinone-2-sulfonic acid sodium salt, $Ru(NH_3)_6Cl_3$, and ferroceneacetic acid were from Sigma-Aldrich. D_2O (99.9% D) and acetic acid-d_4 (99.5% D) were bought from Cambridge Isotope Laboratories, Inc.

Expression and Purification of wt NP7 and NP7(Δ1−3). The proteins were expressed and reconstituted with the heme cofactor as previously described (*45*). The proteins were judged by SDS−PAGE to be ∼90% pure. Proteins were subjected to MALDI-TOF MS to confirm the correct molecular masses, including an initial Met-0 residue in both cases and accounting for two Cys−Cys disulfides (calculated for [*wt* NP7 + H]$^+$ 20 969 Da, observed 20 966 Da; calculated for [NP7(Δ1−3) + H]$^+$ 20 702 Da, observed 20 698 Da). Proteins were stored frozen at −20 °C in 200 mM NaO*Ac*/HO*Ac* and 10% (v/v) glycerol (pH 5.0) until use.

Measurement of Ligand Binding Constants for Fe^{III} Complexes of the Nitrophorins. Association constants were determined by titration experiments at 27 ± 1 °C where absorption spectra where recorded between 325 and 800 nm essentially as described previously (*44*). In the case of NO titrations, all solutions were purged with Ar and a SNAP solution (200 μM in the presence of 50 μM Na_2EDTA) was used as the NO source. To release NO from SNAP (*46*), a few crystals of CuCl were added to the Ar-purged buffer solution and filtered. Protein samples were extensively dialyzed (NMWL, 12−14 kDa) against Ar-purged buffer.

Spectroelectrochemical Titrations. These were carried out using the same instrumentation and the same reference

electrode (Ag/AgCl, $E° = -205$ mV versus SHE) at 27 ± 1 °C as described previously (*16*, *28*, *44*). Protein samples were rendered essentially O_2 free by dialysis (NMWL, 12−14 kDa) in Ar-purged buffer overnight. Methyl viologen, anthraquinone-2-sulfonic acid, and $Ru(NH_3)_6Cl_3$ (in the case where no ligand was added or histamine was bound) or anthraquinone-2-sulfonic acid, $Ru(NH_3)_6Cl_3$, and ferrocene-acetic acid (with NO bound which was added as SNAP) were used as electrochemical mediators at concentrations of ∼200 μM (*16*, *28*). Measurements were performed with either no ligand or a sufficiently high concentration of ligand L to ensure full complexation of both oxidation states where SNAP was used as the NO source.

Kinetics of NO Release. Samples of *wt* NP7 or NP7(Δ1−3) (∼10 μM) in 100 mM MOPS/NaOH (pH 7.5) were loaded with a slight excess of sodium (*Z*)-1-(*N*,*N*-diethylamino)-diazen-1-ium 1,2-diolate (DEA/NO). Excess DEA/NO (or its decomposition products) was washed out using a Centricon-10 (Millipore) ultrafiltration device. To observe kinetics, equal volumes of the protein−NO complex and 10 mM imidazole (ImH) dissolved in the same buffer as the protein were rapidly mixed using an Olis stopped-flow RSM 1000 instrument equipped with a water bath-thermostated cuvette holder which was adjusted to 25 ± 1 °C. Absorption changes at 423 nm versus time were fitted with a single exponential using ORIGIN version 7.5 (OriginLab, Inc.). The measurements were repeated a number of times and averaged.

Thermal Stability. Protein samples (∼5 μM) in 30 mM NaH_2PO_4/NaOH (pH 5.5) were placed in a quartz cuvette, and the cuvette was placed in a temperature adjustable cuvette holder in a UV−vis spectrophotometer. Temperatures were adjusted by an external water bath between 20 and 70 °C in steps of ∼5 °C. Temperatures were determined at the cuvette holder and spectra recorded between 300 and 600 nm after the temperature was stable for 5 min.

EPR Spectroscopy. Samples for EPR spectroscopy were concentrated in Biomax ultrafiltration concentrators with a NMWL of 10 kDa (Millipore). After the concentration reached ∼1 mM, buffer was exchanged in the concentrators with 50 mM MOPS/NaOH (pH 7.5). For the preparation of the ferroheme−NO complex, NP7 in 100 mM NaO*Ac*/HO*Ac* (pH 5.0) was first reduced by the addition of 10 mM $Na_2S_2O_4$. The protein was then separated using a 5 mL HiTrap desalting column (Amersham Biosciences) in 100 mM NaO*Ac*/HO*Ac* (pH 5.0). The protein fraction was briefly subjected to excess NO gas and again separated with the HiTrap desalting column in 100 mM NaO*Ac*/HO*Ac* (pH 5.0). EPR spectra were recorded at 4.2 K on a Bruker ESP-300E EPR spectrometer operating at X-band, using a Systron-Donner frequency counter to measure the microwave frequency. Instrument settings included a microwave power of 0.2 mW, a field modulation of 100 kHz, and a modulation amplitude of 4 G.

NMR Spectroscopy. For the buffered NMR solution, exchangeable protons in Na_2HPO_4 and ImH were exchanged against deuterons by three solvation−freeze-dry cycles with D_2O. The pH was then adjusted through titration with acetic acid-d_4 using a standard pH electrode (H_2O); therefore, the buffers are not corrected for the deuterium effect (designated pH*).

wt NP7 and NP7(Δ1−3) in 100 mM NaO*Ac*/HO*Ac* (pH 5.0) were concentrated using Biomax ultrafiltration concentrators (NMWL, 10 kDa) (Millipore). Buffer was exchanged through extensive washing (10 times) with 30 mM Na_2DPO_4/acetic acid-d_4 in D_2O (pH* 5.5 or 7.0, respectively) in the same ultrafiltration devices. NP1 and NP2 samples were prepared from lyophilizates as previously described (*15*, *23*, *24*, *27*). NMR samples finally consisted of 1−2 mM protein solutions. To obtain the low-spin complexes, protein samples were mixed with excess ImD/acetic acid-d_4 solution in D_2O of either pH* 5.5 or 7.0 (final concentration of 20 mM) prior to ultrafiltration. NMR data were collected at 25 °C with the chemical shift referenced to residual water on a Bruker DRX-500 spectrometer operating at a proton Larmor frequency of 499.58 MHz.

Structural Model of NP7. Amino acid sequences of *R. prolixus* NP1−4 were aligned with NP7 using MUSCLE version 3.6[3] (*47*). On the basis of this alignment, a homology model of NP7(G3−S182) was built using the SWISS-MODEL server[4] (*48*, *49*) and DEEPVIEW version 3.7[5] (*50*). The following X-ray structures were used as modeling templates: PDB entry 1T68 (NP2−NO), PDB entry 1PEE (NP2−ImH), PDB entry 1EUO (NP2−H_2O) (*32*), and PDB entry 2A3F (NP2−H_2O). Upon superposition of the NP7 model structure with the NP2−H_2O crystal structure (PDB entry 2A3F), the heme cofactor was manually inserted into the NP7 model and modified to 2,4-dimethyldeuteroporphyrin IX (symmetrical heme). Finally, the structure was manually refined where the GROMOS96 implementation in DEEPVIEW was used for local energy minimization (200 cycles of steepest descents followed by 300 cycles of conjugated gradients). The modeling result was evaluated by WHAT_CHECK[6] (*51*) and PROCHECK[6] (*52*).

Dynamic Light Scattering. The NMR samples of NP2−ImH (∼2 mM, pH* 7.0) and *wt* NP7−ImH (∼2 mM, pH* 5.5) were aligned in the sample holder of a BI-2030AT laser light scattering goniometer (Brookhaven Instruments Inc., Holtsville, NY), 90° to a 5 mW He/Ne laser (632.8 nm; Melles-Griot Corp., Carlsbad, CA). The relative intensity of the Rayleigh scattering was plotted versus the logarithm of the apparent hydrodynamic diameter.

RESULTS

Amino Acid Sequence of NP7. NP1−4 were previously isolated from the saliva of *R. prolixus*, and their N-terminal amino acid sequences were obtained through Edman degradation (*7*). Comparison with the coding DNA revealed the corresponding signal peptides that are cleaved during the export into the salivary gland lumen (*53*). NP7, however, was derived solely from a cDNA library, and the signal peptide sequence was computed using SIGNALP version 2.0 (*38*). From these calculations, NP7 was predicted to contain three additional amino acid residues, ^{1}Leu-Pro-Gly^{3}, at the N-terminus, whereas NP1−4 are all cleaved one residue before Cys-2. An amino acid sequence alignment of NP7 with NP1−4 was performed using the MUSCLE version 3.6 web server[3] and is displayed in Figure 1. In a recent comparative study of three N-terminal forms of NP2, i.e.,

[3] http://phylogenomics.berkeley.edu/cgi-bin/muscle/input_muscle.py/.
[4] http://swissmodel.expasy.org/.
[5] http://swissmodel.expasy.org/spdbv/.
[6] http://swissmodel.expasy.org/workspace/.

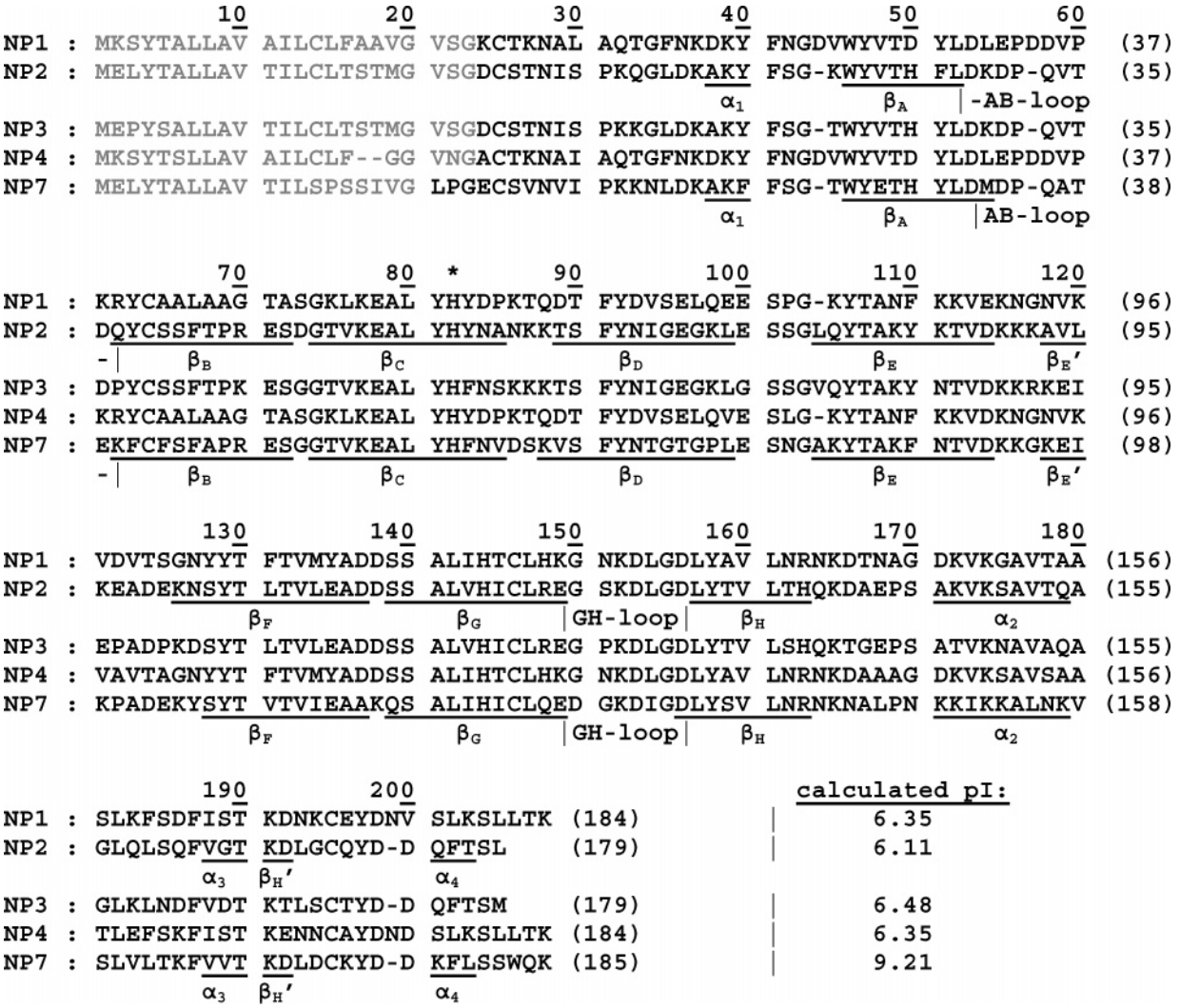

FIGURE 1: Amino acid sequence alignment of *R. prolixus* NP1 (Swiss-Prot entry Q26239), NP2 (Swiss-Prot entry Q26241), NP3 (Swiss-Prot entry Q94733), NP4 (Swiss-Prot entry Q94734), and NP7 (TrEMBL entry Q6PQK2). Signal sequences for secretion are colored gray. The amino acid residue numbering at the end of each line is for the truncated forms throughout this article. The proximal His is indicated with an asterisk. The secondary structure elements, α-helices (α) and *β*-sheets (*β*), are given on the basis of the crystal structure of NP2 (PDB entry 1EUO) (*32*) and the homology model of NP7 and were derived using DEEPVIEW version 3.7 (this work; compare Figure 7). The theoretical p*I* values of the mature proteins (i.e., with truncated signal peptides), taking the two disulfides into account, were calculated at http://www.expasy.ch/tools/pi_tool.html/.

Scheme 1: N-Terminal Amino Acid Sequences of Native and Recombinant *R. prolixus* NP2, NP4, and NP7 and Their N-Terminal Mutants[a]

native:	NP2	: DC...(2)[a]	(*7*)
	NP4	: AC...(2)	(*7*)
recombinant:	NP2	: MDC...(2)	(*44*)
	GSHM-NP2	:GSHMDC...(2)	(*44*)
	NP2(D1A)	: AC...(2)	(*44*)
	NP4	: AC...(2)	(*34*)
	wt NP7	:MLPGEC...(5)	this work
	NP7(Δ1-3)	: MEC...(5)	this work

[a] The numbers in parentheses refer to the positions of the last residues displayed here in the amino acid sequences of the mature proteins (compare to Figure 1).

Met[0]-NP2, NP2(D1A), and $^{-3}$Gly-Ser-His-Met[0]-NP2 (compare Figure 1 and Scheme 1), it was found that even small changes in the N-terminal sequence of *R. prolixus* nitrophorins can have major effects on the protein properties (*44*).

We revisited the prediction of the signal peptidase cleavage site using the SIGNALP web server,[7] the new version (3.0) of which was recently released with improved accuracy (*54*−*56*). In parallel, the signal peptides of NP1−4 were also predicted as a benchmark for the accuracy of the method for *R. prolixus* nitrophorins (Table 1). The neuronal network (NN) approach of SIGNALP version 3.0 predicted the highest probability with a sufficient *D* score (*55*) for the actual sites of NP1−4. For NP1 and NP4, the correct cleavage site was also predicted by the hidden Markov model (HMM) approach; however, for NP2 and NP3, the HMM predicted the maximum probability at different sites (Table 1 and Figure 1). Furthermore, the probability of the presence of the cleavage sites was below the threshold of significance (<0.5). However, for NP7, the signal peptidase cleavage site calculated previously with SIGNALP version 2.0 (*38*) could be verified with good scoring by applying both the NN and HMM approaches (Table 1 and Figure 1). Overall, SIGNALP version 3.0 was able to predict the correct signal peptide cleavage site of *R. prolixus* nitrophorins with reasonable reliability (total accuracy of 75%) for NP1−4, which is close to the proposed accuracy (79.0% for NN and 75.7% for

[7] http://www.cbs.dtu.dk/services/SignalP/.

Table 1: Computational Prediction of the Signal Peptide Cleavage Site of *R. prolixus* Nitrophorins Using SignalP Version 3.0 (Program Described in Refs *54*−*56*)

	NP1	NP2	NP3	NP4	NP7
NN[a]	0.840	0.783	0.776	0.930	0.609
HMM[b]	0.814	0.339[c]	0.339[d]	0.980	0.845
cleavage site[e]	VSG^{23} | $K^{24}CT$	VSG^{23} | $D^{24}CS$	VSG^{23} | $D^{24}CS$	VNG^{21} | $A^{22}CT$	IVG^{20} | $L^{21}PG$

[a] *D* score for the predicted cleavage site using the neuronal network (NN) approach. [b] Maximum cleavage site probability for the hidden Markov model (HMM) approach. [c] In this case, the highest probability (0.473) was determined for the cleavage at TMG^{20} | $V^{21}SG$. [d] In this case, the highest probability (0.468) was determined for the cleavage at TMG^{20} | $V^{21}SG$. [e] The part of the amino acid sequence where the cleavage was proposed to occur. In contrast to the rest of the article, the numbering of residues in this table refers to the start of translation of the genes in the insect (compare to Figure 1).

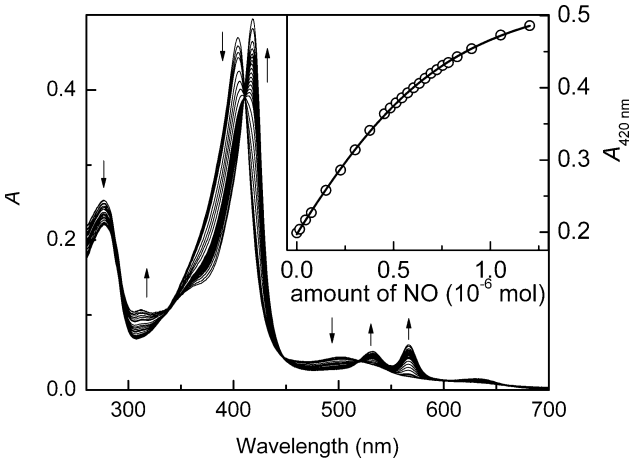

FIGURE 2: Titration of *wt* NP7 from *R. prolixus* in 100 mM MOPS/NaOH (pH 7.5) with NO at 25 ± 1 °C. SNAP was used as an NO donor, and the presence of Cu^{I} ions catalyzed the immediate decomposition of the *S*-nitrosothiol SNAP according to the reaction 2R-S-N═O → R-S-S-R + 2NO.

HMM) (*55*). Thus, the prediction of the cleavage site for NP7 by both the NN and HMM approaches with rather high scoring in both cases (Table 1) seems reliable but not totally without doubt. In view of the previous results on the differences in N-terminal NP2 variants (*44*), we decided to characterize NP7 with the first three amino acids (designated *wt* NP7) and the truncated form [designated NP7(Δ1−3)]. The recombinant expression of both proteins was accomplished in good yield in *Escherichia coli* cells. As for NP1−3, due to the recombinant expression of nitrophorins in *E. coli*, a Met-0 residue was added to the amino acid sequence in the case of NP7 and NP7(Δ1−3) that results from the translation of the start codon 5′-ATG-3′ (Scheme 1). The presence of Met-0 was affirmed by mass spectrometry.

Association Constants of NO and Histamine. Like NP1 (*13*), NP7 released NO at pH 7.5 when Ar was blown over the sample surface while the oxidation state was maintained at +3 (*45*). To compare the affinity of NP7 for NO with those of the other nitrophorins, association constants K_{eq}^{III} for binding of NO to ferric *wt* NP7 and NP7(Δ1−3) were determined by titrations at pH 5.5 and 7.5 (*44*). Figure 2 gives an example of the titration of *wt* NP7 with NO at pH 7.5, which shows good isosbestic behavior. The resulting values are summarized in Table 2 in comparison to the reported values for NP1−4 and several NP2 mutant proteins relevant to this study (*21*, *28*). Like the other *R. prolixus* nitrophorins, *wt* NP7 binds NO at low pH very tightly and switches to a lower affinity at serum pH. In fact, in the case of *wt* NP7, this switch of the association constant is the largest observed among the nitrophorins (2−3 orders of magnitude). This difference is a prerequisite for nitrophorin function. It is, however, the largest difference in K_{eq}^{III}(NO) between the two pH values observed for any nitrophorin. In marked contrast, NP7(Δ1−3) exhibited the largest K_{eq}^{III}(NO) at plasma pH, suggesting that this protein would not be capable of releasing NO in blood plasma, while opposite to the general trend, the K_{eq}^{III}(NO) at pH 5.5 drops approximately 1 order of magnitude.

NP1−4 aid the insect not only by NO release but also by trapping histamine at the open Fe^{III} coordination site to suppress the victim's immune response (*19*). Because the human plasma concentration of histamine is relatively small ($1-10 \times 10^{-9}$ M) (*57*), the K_{eq}^{III}(Hm) values of NP1−4 at pH 7.5 are in the range of $\sim 10^8$ M^{-1} (Table 2), to trap significant amounts of histamine (*21*, *28*). In marked contrast, NP7 exhibits a 3 order of magnitude smaller association constant (Table 2), suggesting that this protein is not able to sequester histamine in vivo. To investigate further if the lower histamine affinity is a matter of the specific heme properties of NP7 and/or the NP7 polypeptide chain, K_{eq}^{III} was also determined for ImH. It turned out that ImH binds with a similar affinity to *wt* $NP7^{III}$ and $NP1-4^{III}$ (Table 2); therefore, it is concluded that the difference between ImH and histamine is caused by the additional ethylammonium moiety of histamine. In fact, in the NP4−Hm X-ray structure at pH 5.6 (PDB entry 1IKE) (*35*) and the NP1−Hm X-ray structure at pH 7.5 (PDB ebtry 1NP1) (*31*), histamine:NH_3^+ was hydrogen bonded to Asp-30:$C^{\gamma}OO^-$ and the backbone C═O group of Gly-131. In the case of the NP1−Hm complex, further hydrogen bonding to the backbone C═O groups of Glu-32 and Leu-130 occurred. Mutation of Asp-30 in NP4 to Asn or Ala significantly decreased histamine association constants (*30*). Likewise, mutation of the equivalent residue Asp-29 to Ala in NP2(D1A) also decreased the histamine association constant at pH 7.5 by 10^2-10^3 M^{-1}, whereas the ImH association constants remained nearly unchanged (R. E. Berry, M. N. Shokhirev, A. Y. W. Ho, H. Zhang, and F. A. Walker, manuscript to be submitted) (Table 2). Moreover, X-ray crystallography of NP4 showed that those residues involved in histamine:NH_3^+ binding are embedded in a larger hydrogen bonding network in which the N-terminal C^{α}-NH_3^+ group (Ala-1) is strongly involved (*30*). Consequently, elongation of the N-terminus could have an influence on the histamine binding affinity. This hypothesis is supported by the fact that NP7(Δ1−3), in contrast, resulted in an increased K_{eq}^{III}(Hm) comparable to those of NP1−4 (Table 2), thus indicating that the opening of the heme pocket is indeed influenced by the N-terminus. However, in contrast to NP7, the N-terminal variants of NP2 did not show significant differences regarding histamine binding, which supports the idea that the N-terminus of *wt* NP7 is somewhat unique in that ability to decrease histamine affinity.

Table 2: Association Constants (K_{eq}) of the Distal Heme Ligands L = NO, Histamine, and ImH for Binding to *wt* NP7 and NP7(Δ1−3) at 25 ± 1 °C in Comparison to the Data Reported for *R. prolixus* NP1−4

	$\log_{10} K^{III}_{eq}$ ($\log_{10}$ M^{-1})[a]				$\log_{10} K^{II}_{eq}$ ($\log_{10}$ M^{-1})[b]		
	NO		histamine	ImH	NO		histamine
	pH 7.5	pH 5.5	pH 7.5	pH 7.5	pH 7.5	pH 5.5	pH 7.5
NP1	6.1 ± 0.1[c]	6.92[c]	8.0 ± 0.2[d]	6.85[d]	13.3[d]	14.1[d]	6.36[d]
NP2	8.3 ± 0.1[e]	~9.0[c]	8.0 ± 0.1[d]	7.4 ± 0.1[d]	13.6[e]	~14.6[d]	5.2[d]
NP2(D1A)	8.3 ± 0.1[e]		8.0 ± 0.2[e]	7.4 ± 0.1[e]	13.4[e]		6.0[e]
GSHM-NP2	8.4 ± 0.1[e]		8.0 ± 0.1[e]	7.2 ± 0.1[e]	13.6[e]		6.5[e]
NP2(D1A,D29A)	8.0 ± 0.2[f]		5.5 ± 0.4[f]	6.8 ± 0.1[f]	13.3[f]		
NP3	7.0 ± 0.2[g]		7.60[d]	7.69[d]			6.46[d]
NP4	6.92[c]	7.30[c]	8.18[d]	6.85[d]	−	13.23[d]	6.06[d]
wt NP7[h]	6.6 ± 0.1	>9	5.0 ± 0.1	6.0 ± 0.1	13.0	>14	4.1
NP7(Δ1−3)[h]	~9.0	8.2 ± 0.1	7.1 ± 0.1	7.5 ± 0.1	>15	12.7	5.9

[a] Association constants of the ferric state of the indicated nitrophorin. [b] Association constants of the ferrous state of the indicated nitrophorin. These values were calculated from K^{III}_{eq} in combination with the reduction potentials reported in Table 3 according to eq 1. [c] From ref *28*; determined in 40 mM Tris/HCl (pH 8.0) or 40 mM NaO*Ac*/HO*Ac* (pH 5.0). [d] From ref *21*; determined in 100 mM NaH_2PO_4/NaOH (pH 7.5 or 5.5). [e] From ref *44*; determined in 100 mM NaH_2PO_4/NaOH (pH 7.5 or 5.5). [f] R. E. Berry, M. N. Shokhirev, A. Y. W. Ho, H. Zhang, and F. A. Walker, manuscript to be submitted; determined in 100 mM NaH_2PO_4/NaOH (pH 7.5 or 5.5). [g] This work; determined in 100 mM NaH_2PO_4/NaOH (pH 7.5 or 5.5). [h] This work; determined in 100 mM MOPS/NaOH (pH 7.5) or 100 mM NaH_2PO_4/NaOH (pH 5.5).

Table 3: Standard Reduction Potentials ($E°$) of *R. prolixus wt* NP7 and NP7(Δ1−3) at 27 ± 1 °C in Complex with the Distal Heme Ligand L, in Comparison to the Data Reported for NP1−4[a]

		E^o_c (mV versus SHE)			$E^o_c - E^o_{H_2O}$ (mV)	
		H_2O[b]	NO	histamine	NO	histamine
NP1	pH 5.5	−274 ± 2[c]	+154 ± 5[c]	−339 ± 2[d]	+428	−65
	pH 7.5	−303 ± 4[c]	+127 ± 4[c]	−403 ± 1[d]	+430	−100
NP2	pH 5.5	−287 ± 5[d]	+49 ± 3[d]	−410 ± 3[d]	+336	−123
	pH 7.5	−310 ± 5[d]	+8 ± 3[d]	−474 ± 5[e]	+318	−142
NP2(D1A)	pH 5.5	−318 ± 2[f]	+48 ± 2[f]	−408 ± 2[f]	+366	−90
	pH 7.5	−325 ± 4[f]	−20 ± 2[f]	−440 ± 3[f]	+305	−115
GSHM-NP2	pH 7.5	−360 ± 5[f]	−15 ± 3[f]	−451 ± 3[f]	+345	−91
NP3	pH 5.5	−321 ± 5[d]	+73 ± 1[e]	−339 ± 2[e]	+394	−18
	pH 7.5	−335 ± 1[d]	+13 ± 1[e]	−403 ± 1[e]	+348	−68
NP4	pH 5.5	−259 ± 2[d]	+94 ± 5[d]	−393 ± 2[d]	+353	−134
	pH 7.5	−278 ± 4[d]	−[g]	−404 ± 1[d]	−	−126
wt NP7[h]	pH 5.5	−253 ± 5	+94 ± 5	−254 ± 5	+346	−1
	pH 7.5	−268 ± 4	+109 ± 7	−319 ± 8	+377	−51
NP7(Δ1−3)[h]	pH 5.5	−109 ± 6	+157 ± 3	−225 ± 6	+266	−116
	pH 7.5	−182 ± 5	+228 ± 4	−254 ± 6	+410	−72
$E^o_{NP7(\Delta1-3)} - E^o_{wt\ NP7}$	pH 5.5	+144	+63	+29		
	pH 7.5	+86	+119	+65		

[a] Except where noted, all were measured in 100 mM NaH_2PO_4/NaOH (pH 5.5 or 7.5). [b] No ligand added. [c] From ref *16*. [d] From ref *28*. [e] From ref *21*. [f] From ref *44*. [g] This value could not be measured because of facile dissociation of NO (*28*). [h] This work; determined in 100 mM MOPS/NaOH (pH 7.5) or 100 mM NaH_2PO_4/NaOH (pH 5.5).

Because of the high affinity of NO for Fe^{II} centers, K^{II}_{eq}(NO) is difficult to measure directly. However, the shift of the Fe^{III}/Fe^{II} reduction potential when a ligand L is bound to the iron is a measure of the ratio of the Fe−L binding constants for the two oxidation states, since the Nernst equation (eq 2, see below) can be rewritten as

$$E^o_c - E^o = \frac{RT}{nF} \ln \frac{K^{III}_{eq}(L)}{K^{II}_{eq}(L)} \quad (1)$$

where E^o_c is the measured potential for the nitrophorin fully complexed to the ligand L in both oxidation states, $E°$ is the measured potential for the nitrophorin in the absence of L, R is the gas constant, T is the temperature, n is the number of electrons involved (=1), F is the Faraday constant, and K^{III}_{eq}(L) and K^{II}_{eq}(L) are the association constants for association of ligand L with the Fe^{III} and Fe^{II} states, respectively. Thus, the combination of the two reduction potentials $E°$ and E^o_c (see the next section) together with K^{III}_{eq}(L) allowed the calculation of K^{II}_{eq}(L) values, which are reported in Table 2 as well. The low histamine affinity of *wt* $NP7^{III}$ compared to that of $NP7(\Delta1-3)^{III}$ and the other ferric nitrophorins is reflected also by an extraordinarily low K^{II}_{eq}(Hm).

Similarly, the large difference in K^{III}_{eq}(NO) of *wt* NP7 between pH 5.5 and 7.5 is also reflected in the corresponding K^{II}_{eq}(NO). Remarkably, the calculated K^{II}_{eq}(NO) values for NP7(Δ1−3) resemble not only the lowest NO affinity at pH 5.5 but also the highest NO affinity at pH 7.5 among all NP^{II} species reported, indicating that other factors besides the iron oxidation state strongly influence the Fe^{II}−NO bond.

Spectroelectrochemical Titrations. Spectroelectrochemical titrations of NP7 and NP7(Δ1−3) were performed at low and high pH with H_2O, NO, and histamine as ligands (Table 3). Figure 3 shows the measurement of the reduction potential

of the *wt* NP7−Hm complex at pH 7.5 as an example. The reduction potentials ($E°$) were derived from the fitting of the spectroscopic change at a single wavelength according to the Nernst equation

$$E^{o}_{app} = E^{o} + 2.303\frac{RT}{nF}\log_{10}\frac{[NP^{III}]}{[NP^{II}]} \quad (2)$$

where E^{o}_{app} is the applied potential and [NP^{III}] and [NP^{II}] are the equilibrium concentrations of ferric and ferrous NP, respectively, which can be determined from the absorption spectra at each applied potential by using Beer's law. The resulting values are summarized and compared to those of NP1−4 in Table 3. Overall, the values obtained for *wt* NP7 are generally higher, but still close to those of the other isoforms. However, NP7−H_2O and NP7−Hm complexes exhibit the highest $E°$ at both pH values, and these values are topped only by those of NP1−NO complexes (by +60 mV at pH 5.5 and +18 mV at pH 7.5). Thus, the Fe^{III} oxidation state tends to be less stabilized in NP7 than in NP1−4.

The picture is more dramatic for NP7(Δ1−3) where all reduction potentials were found to be positively shifted on average +85 mV as compared to that of the *wt* (Table 3). This is an unprecedented shift resulting from a seemingly mild modification. For comparison, $^{-3}$Gly-Ser-His-Met^{0}-NP2 exhibited an only marginal (+23 mV) change compared to *wt* NP2 (*44*). This again points to an important role of the N-terminal sequence of NP7 for its functionality.

Whereas the reduction of the NP7−NO complex at pH 7.5 resulted in a slight shift of the Soret band from 414 nm ($NP7^{III}$−NO) to 411 nm ($NP7^{II}$−NO) and reduction of the NP7−NO complex at pH 5.5 in the spectroelectrochemical cell resulted in a broad Soret band maximum at ∼380 nm (Figure 4A), which is indicative of a switch to a five-coordinate (protein ligand off) nitrosyl complex. Upon reoxidation, the Soret maximum was restored to the initial value of 419 nm; i.e., the six-coordinate Fe^{III}−NO complex was re-formed. To prove that indeed a five-coordinate Fe^{II}−NO species was formed at low pH, the EPR spectrum of a NP7−NO sample reduced with $Na_2S_2O_4$ at pH 5.0 was recorded (Figure 4B). The resulting spectrum with a g_{iso} of 2.01 and the ^{14}N hyperfine splitting ($I = 1$) is typical for a five-coordinate ferroheme nitrosyl (*58*−*60*). In contrast to *wt* NP7, NP7(Δ1−3) showed the formation of a five-coordiante Fe^{II}−NO species upon reduction at pH 7.5 (Figure 4C), but not at pH 5.5. This reverse pH behavior has not previously been observed for any other *R. prolixus* nitrophorin.

Kinetics of NO Release. The reaction between ferric nitrophorins and NO can be described by the equilibrium reaction depicted in Scheme 2.

The reaction is described by the simple equation

$$k_{obs} = k_{on}[NO] + k_{off} \quad (3)$$

where [NO] is the NO concentration, k_{off} is the reverse rate constant (or dissociation constant), and k_{on} is the second-order rate constant for NO binding. Both k_{off} and k_{on} can be determined from the association reaction by measuring k_{obs} at various NO concentrations. However, k_{off} values determined by this experiment for systems with very large

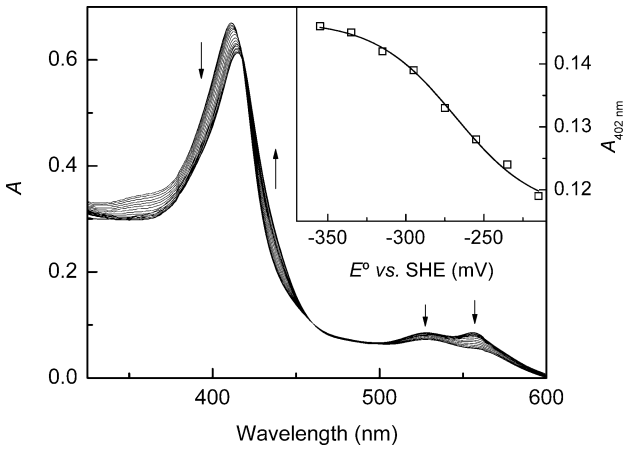

FIGURE 3: Electrochemical titration of the *wt* NP7−Hm complex in 100 mM MOPS/NaOH (pH 7.5) at 27 ± 1 °C in the presence of the electrochemical mediators methyl viologen, anthraquinone-2-sulfonic acid, and $Ru(NH_3)_6Cl_3$ (each ∼200 μM).

Scheme 2

$$NP^{III} + NO \underset{k_{off}}{\overset{k_{on}}{\rightleftharpoons}} NP^{III}{-}NO$$

Scheme 3

$$NP^{III}{-}NO + ImH \underset{k_{on}}{\overset{k_{off}}{\rightleftharpoons}} NP^{III} + NO + ImH \xrightarrow{k^{ImH}} NP^{III}{-}ImH + NO$$

association constants ($K_{eq} = k_{on}/k_{off}$) are unreliable, and the reverse rate constant that is obtained represents the dissociation of NO from the unstabilized pre-equilibrated Fe^{III}−NO complex (*28*). Rather, the dissociation rate constant (k_{off}) for the release of NO from the equilibrated Fe^{III}−NO complex was determined independently by measuring the rate of the displacement reaction by ImH according to Scheme 3.

For this purpose, *wt* NP7 or NP7(Δ1−3) (∼10 μM) was loaded with NO as described in Experimental Procedures and then rapidly mixed in a quartz cuvette with an equal volume of buffer containing 10 mM ImH. The displacement reaction was followed at 423 nm using a stopped-flow spectrophotometer for which a representative experiment is shown in Figure 5. The displacement reaction shown in Scheme 3 can be described by the following equation

$$k_{obs} = \frac{k_{off}}{1 + \dfrac{k_{on}[NO]}{k^{ImH}[ImH]}} \quad (4)$$

where k_{obs} is the observed first-order displacement rate constant, k_{off} is the NO dissociation rate constant, k_{on} is the bimolecular rate constant for NO binding, [ImH] is the imidazole concentration, k^{ImH} is the bimolecular rate constant for ImH binding, and [NO] is the NO concentration. In this NO displacement experiment, [NO] ≪ [ImH]. Thus, the rate of NO association is insignificant, and NO displacement is rate-determining. Under these conditions, eq 4 simplifies to $k_{obs} = k_{off}$. The resulting absorption traces were fit with a single exponential that resulted in a good fit for both proteins (as shown by the residuals in Figure 5 for *wt* NP7). The average k_{off} values from a number of repeated experiments are given in Table 4 together with the corresponding k_{on} values which were calculated from the association constants given in Table 2 ($K_{eq} = k_{on}/k_{off}$).

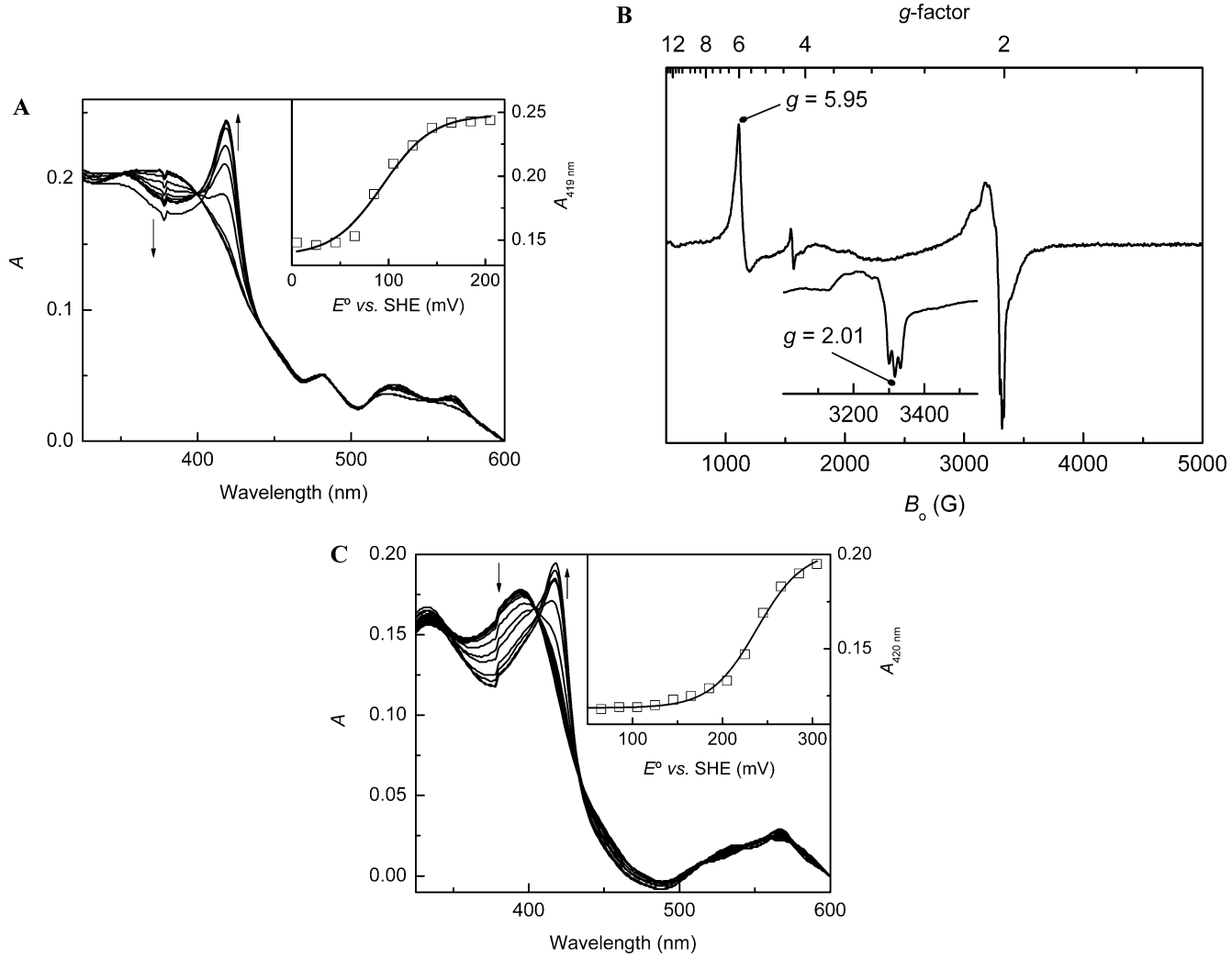

FIGURE 4: Spectroelectrochemistry and EPR spectroscopy of NP7−NO complexes. (A) UV−visible spectra of the *wt* NP7−NO complex in 100 mM NaH_2PO_4/NaOH (pH 5.5) as a function of applied potential (−200, −180, −160, −140, −120, −100, −80, −60, −40, −20, and 0 mV versus Ag/AgCl; add 205 mV for potential versus SHE). The inset shows a fit of the spectroelectrochemical data. (B) EPR spectrum of the *wt* $NP7^{II}$−NO complex in 50 mM NaO*Ac*/HO*Ac* (pH 5.0) recorded at 4.2 K at X-band. Other than a small amount of high-spin Fe^{III} ($g_{||}$ = 5.95) originating from unligated NP7, the signal is characteristic of five-coordinate Fe^{II}−NO heme centers (g_{iso} = 2.01; see the inset for detailed resolution) (*58*, *59*). (C) UV−visible spectra of the NP7(Δ1−3)−NO complex in 100 mM MOPS/NaOH (pH 7.5) as a function of applied potential (−140, −120, −100, −80, −60, −40, −20, 0, +20, +40, +60, +80, and +100 mV versus Ag/AgCl; add 205 mV for potential versus SHE). The inset shows a fit of the spectroelectrochemical data.

Interestingly, k_{off} values for *wt* NP7 and NP7(Δ1−3) are similar, but k_{on} values are significantly different from each other as a consequence of very different K_{eq} values. In comparison to that of NP1−4 (*28*) (Table 4), the k_{off} decreases in the following order: NP1/4 > NP7 > NP2/3. The k_{on} for *wt* NP7 appears to be similar to those of NP1/4, but the very fast k_{on} for NP7(Δ1−3) is very different from any of the other nitrophorin values; thus, the ^{0}Met-Leu-Pro-Gly^3 N-terminus strongly contributes to k_{on} rather than k_{off}. It should be noted that biphasic reaction kinetics were reported for NP1/4 and for NP2/3 to a lesser extent (*28*), but in this work, only one phase could be observed for NP7. The two different rates for NP1/4 have been attributed to the two different heme *b* orientation isomers (*44*), and since NP7 is dominated by the **A** heme orientation (see below), it is not surprising that the amplitude due to a second, slow phase is too small to observe. Therefore, in this study, only the fast phase, which is the major fraction of the reaction, was used for comparisons.

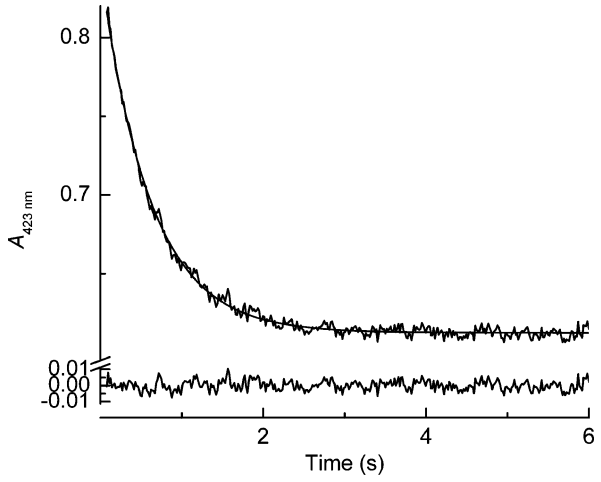

FIGURE 5: Stopped-flow kinetic measurement of the ImH displacement of NO bound to *wt* NP7 in 100 mM MOPS/NaOH (pH 7.5) at 25 °C. Absorption at 423 nm was monitored, and the data (black) were fitted with a first-order model (gray). The residual is displayed at the bottom.

Table 4: Kinetic Parameters for Binding of NO to Ferric *R. prolixus wt* NP7 and NP7(Δ1−3) in Comparison to Those of NP1−4 at High pH

	k_{off} (s^{-1})	k_{on} ($\times 10^6$ M^{-1} s^{-1})
NP1[a]	2.2 ± 0.1	1.5 ± 0.1
NP2[a]	0.12 ± 0.01	33
NP3[b]	0.08 ± 0.01	6.7
NP4[a]	2.6 ± 0.1	2.3
wt NP7[c]	0.606 ± 0.13	2.4[d]
NP7(Δ1−3)[c]	0.50 ± 0.02	∼500[d]

[a] Determined in 40 mM Tris/HCl (pH 8.0) at 25 °C; taken from ref *28*, where k_{off} is termed the fast rate k_{off1} and k_{on} the fast rate k_1. [b] Determined in 40 mM Tris/HCl (pH 8.0) at 12 °C; taken from ref *28*, where k_{off} is termed the fast rate k_{off1} and k_{on} the fast rate k_1. [c] Determined in 100 mM MOPS/NaOH (pH 7.5) at 25 ± 1 °C (this work). [d] Calculated from $K_{eq} = k_{on}/k_{off}$, where K_{eq}^{III} was taken from Table 2.

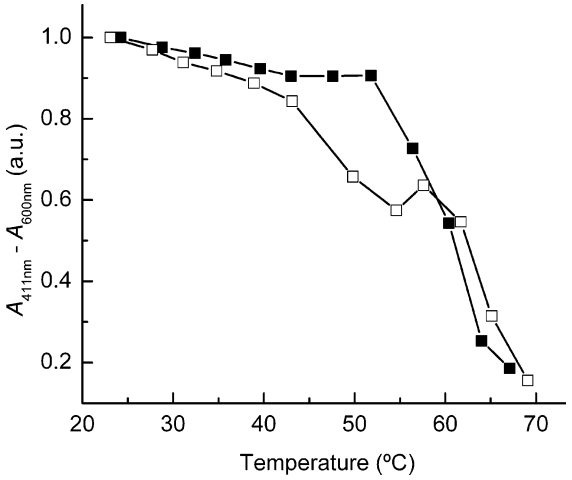

FIGURE 6: Thermal stability of *wt* NP7−ImH (■) and NP7(Δ1−3)−ImH (□) complexes in 30 mM NaH_2PO_4/NaOH (pH 5.5). The temperature was increased in ∼5 °C steps, and then the sample equilibrated for 5 min after the temperature was reached. Subsequently, absorption spectra were recorded between 300 and 600 nm. To account for the formation of precipitate at higher temperatures, the apparent absorption at 600 nm was subtracted from the absorption at 411 nm and the difference values were plotted versus temperature.

Protein Stability. To study the influence of the N-terminus on the stability of NP7, the temperature dependence on the fold stabilization of *wt* NP7 and NP7(Δ1−3) was studied. Increasing light scattering at temperatures of ≥60 °C (for *wt* NP7) and ≥55 °C [for NP7(Δ1−3)] indicated protein aggregation, which did not allow refolding. The Soret absorbance at 411 nm was plotted versus temperature for both proteins upon subtraction of the absorbance at 600 nm which partly accounted for the increased light scattering at higher temperatures (Figure 6). The Soret absorbance constantly decreased with an increase in temperature in the case of NP7(Δ1−3) until at ∼45 °C a marked absorbance decay occurred and was accompanied by Soret band broadening and a shift of the maximum to a shorter wavelength. *wt* NP7, in contrast, was comparatively stable and did not experience a marked signal decrease below 52 °C. Thus, it can be concluded that the N-terminus of NP7 significantly stabilizes the protein fold.

Attempts to observe the difference in fold stabilization free energy (ΔG_f^o) were made by using guanidinium chloride titration experiments, which have been successfully performed in the case of other heme *b* proteins such as horse heart Mb (*61*) and cytochrome b_{562} (*62*). However, due to the irreversibility of the process at both pH 7.0 and 5.0, proper data analysis was not possible.

Scheme 4: Chemical Structure and Numbering of the **A** and **B** Heme Orientations in *R. prolixus* NP2[a]

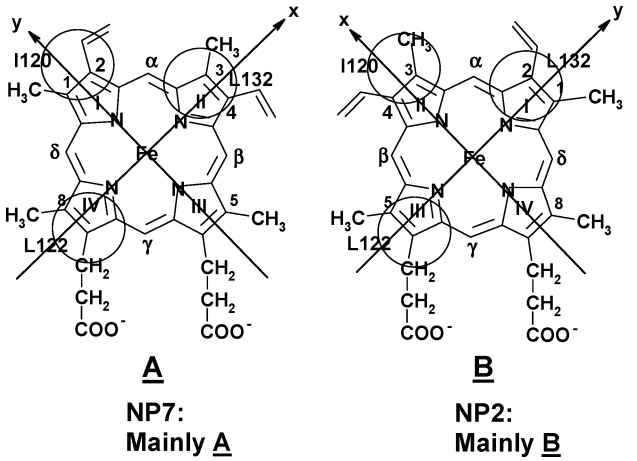

[a] The view is from above the distal side, with His-57 behind the heme. Substituents on the periphery of the heme are numbered clockwise from 1-CH_3 to 8-CH_3 for the **A** orientation and counterclockwise for the **B** orientation. Circles denote the position of three distal side chains that point onto the heme plane in the approximate positions shown (*15*, *32*).

Homology Model of NP7. To examine the structural properties of the heme cavity as well as to attempt to rationalize the strong influence of the N-terminus, a homology model of NP7 was built. The amino acid sequence of NP7 is 61% identical to that of NP2 without any gap in the sequence alignment (Figure 1). This allowed the calculation of a reliable homology model of NP7(G3−S182), which was based on the crystal structures of ferric NP2−H_2O, NP2−NO, and NP2−ImH complexes. Because of the asymmetry of the heme *b* cofactor, it can be inserted in two different orientations, **A** and **B**, into a protein's heme binding pocket. In the protohemin IX drawings of Scheme 4, the **A** isomer is defined as having pyrrole ring II (including 4V) lying above the protein backbone C(O)CN(H) atoms of His-57 (NP2), His-59 (NP1 and NP4), or His-60 (NP7) with that His ligand lying behind the plane of the heme in the pictures shown in Scheme 4. The heme *b* cofactor from the NP2−H_2O crystal structure was manually inserted into the NP7(GS−S182) model structure and then modified into 2,4-dimethyldeuteroporphyrin IX (symmetrical heme) to allow heme seating to be independent of the placement of the vinyl-β carbons that account for the heme **B** orientation in the NP2 structure in contrast to the preferential heme **A** orientation found in NP7 (see below). The NP7(G3−S182) model structure had a rmsd of 0.39 Å compared to the NP2−H_2O complex (based on the superposition of 720 atoms) and showed the same lipocalin type of fold (globular; diameter of ∼40 Å) as the other *R. prolixus* NPs, as shown in Figure 7A (Ramachandran plot: favored 87.7%, allowed 12.3%, generally allowed 0.0%, disallowed 0.0%).

In the previous report on NP7, a homology model was presented that showed the highly positively charged site opposite the heme pocket due to spatial clustering of a large number of Lys residues, and that this site accounts for the recognition of negatively charged membrane surfaces (*38*). Because we noticed the strong influence of the N-terminus

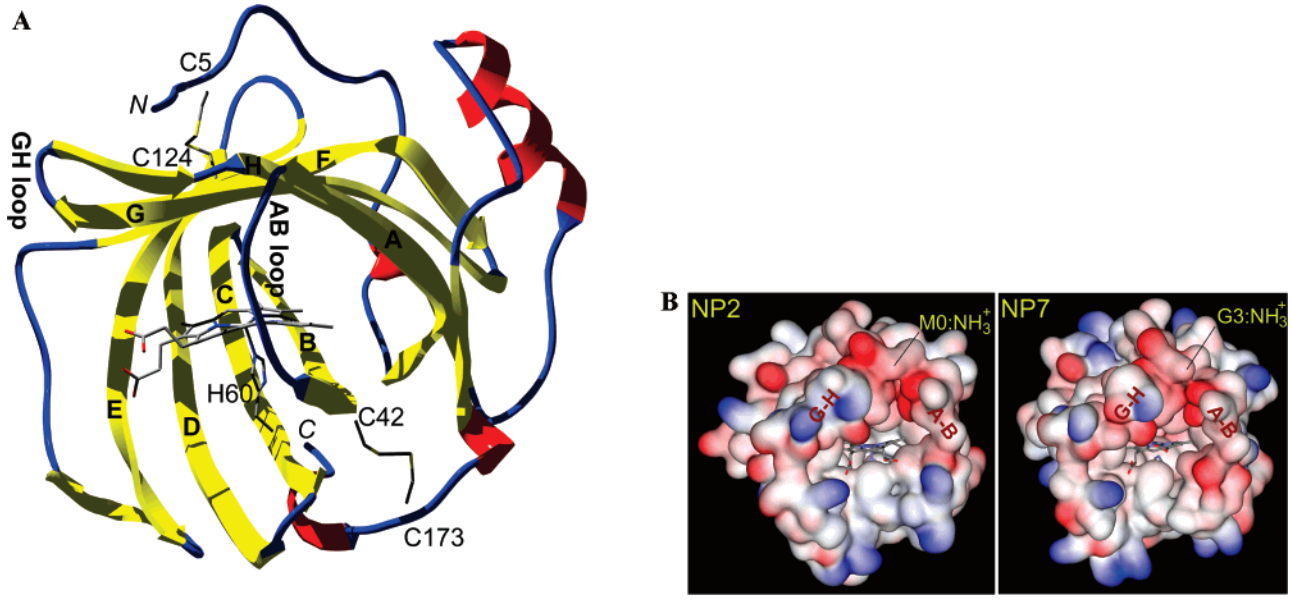

FIGURE 7: Homology model of NP7(G3−S182) from *R. prolixus* with 2,4-dimethyldeuteroporphyrin (symmetrical heme) based on the crystal structure of NP2 (rmsd = 0.39 Å) and on the sequence alignment given in Figure 1. (A) Ribbon diagram of the NP7(G3−S182) homology model. In agreement with Figure 1, the main β-strands are designated A to H in bold letters and the A−B and G−H loops are mentioned. The N- and C-termini are designated with italic letters. The four disulfide-forming Cys residues, the heme cofactor, and the proximal His-60 are displayed as stick models. (B) Surface representations of the heme entrance site of (left) NP2 (PDB entry 1EUO) (*32*) and (right) the homology model of NP7(G3−S182) (this work). The molecules are oriented 90° counterclockwise compared to panel A. The surface electrostatic potential is colored blue (positive) and red (negative). The heme and the proximal His were left out of the surface calculation and are displayed individually as stick models. Figures were prepared with DEEPVIEW version 3.7 and rendered with POV-RAY version 3.6 (http://www.povray.org) (A) or VIEWERLITE version 5.0 (B).

on the NP7 functionality, we were interested in the charge distribution of the surface of the heme entrance site that is close to the N-terminus. The surface representation of the electrostatic potentials of the heme pocket site of NP7(G3−S182) in comparison to NP2 is displayed in Figure 7B. It shows that the heme pocket site is mostly negatively charged, but unlike the case for the site opposite of the heme entrance (*38*), no significant surface charge differences between the two structures were noticed in the area of the N-terminus.

Magnetic Resonance Spectroscopy. The $NP7^{III}$−ImH and $NP7(\Delta1-3)^{III}$−ImH complexes at pH 7.5 exhibited typical rhombic EPR spectra with g_x, g_y, and g_z values of 1.36, 2.19, and 3.07 and 1.38, 2.18, and 3.08, respectively, which are comparable to those of $NP2^{III}$−ImH [1.37, 2.26, and 3.02 (*15*)] and $NP4^{III}$−ImH [1.46, 2.25, and 3.02 (*21*)] complexes. The comparison of the crystal structures with the EPR spectra of bis(ligand) ferriporphyrin model compounds, e.g., *paral*-[Fe(octamethyltetraphenylporphyrin)(1-methylimidazole)$_2$]-Cl, revealed that such a normal rhombic spectrum is indicative of an approximately parallel axial ligand orientation (i.e., His-60|ImH) (*15*, *63*).

The ^{1}H hyperfine-shifted resonances of the ImH complex of *wt* NP7 and NP7(Δ1−3) in comparison to NP2 in buffered D_2O are shown in Figure 8. Reasonably sharp resonances for NP7 could only be obtained at low pH. However, the heme resonances of the other nitrophorins have much smaller average linewidths, $\Delta\nu$ (*23*). Figure 8 shows as an example the spectra of the NP2−ImH complex at high and low pH; i.e., $\Delta\nu$ = 89 Hz at pH 7.0 and 96 Hz at pH 5.5, whereas for *wt* NP7 $\Delta\nu$ = 282 Hz and for NP7(Δ1−3) $\Delta\nu$ = 179 Hz. The number of heme resonances indicates that, unlike many other noncovalently bound heme *b*-containing proteins such as cytochromes b_5 (*64*, *65*), one orientation of the unsymmetrical heme group is strongly favored. This result is consistent with the results of the other *R. prolixus* nitrophorins where equilibrium was reached between the **A** and **B** orientations of heme *b*, e.g., for the NP1−ImH complex after 12 h (*16*). The heme resonances of the NP1−ImH and NP2−ImH complexes at pH 7.0 were previously fully assigned (*23*), and part of the assignment is given in Figure 8. Recording the spectra of the NP2−ImH complex at pH 5.5 obviously yielded moderate shifts of some of the resonances, but the relative position of the signals remained similar, allowing the conclusion that the influence of the pH on the ImH and proximal His-57 orientation in NP2 may be only minor (F. Yang and F. A. Walker, manuscript to be submitted). However, the appearance of small resonances at lower shielding was noticed; these may be due to reorientation of heme in the pocket to increase the amount of isomer **A** as compared to **B** and/or another ImH plane orientation of isomer **B**. On the basis of the previous studies of NP2 (*24*), NP1 and NP4 (*22*, *23*), and NP3 (*27*), we know that the **B** isomer is either equal in abundance to or much more abundant than the **A** isomer in all these cases (Scheme 4).

The ^{1}H NMR spectra of the *wt* NP7−ImH and NP7(Δ1−3)−ImH complexes are very similar to each other, which indicates a very similar chemical environment for the hemes in the two proteins, and a minimal effect of the N-terminal sequence on the shape of the heme binding pocket. The small differences between the spectra of the *wt* NP7−ImH and NP7(Δ1−3)−ImH complexes are surprising considering the strong influences of the N-terminal sequence on the protein functionality that we are reporting. However, in comparison to the other nitrophorins, the spectra of both are very different. The shift to lower shielding is the largest observed

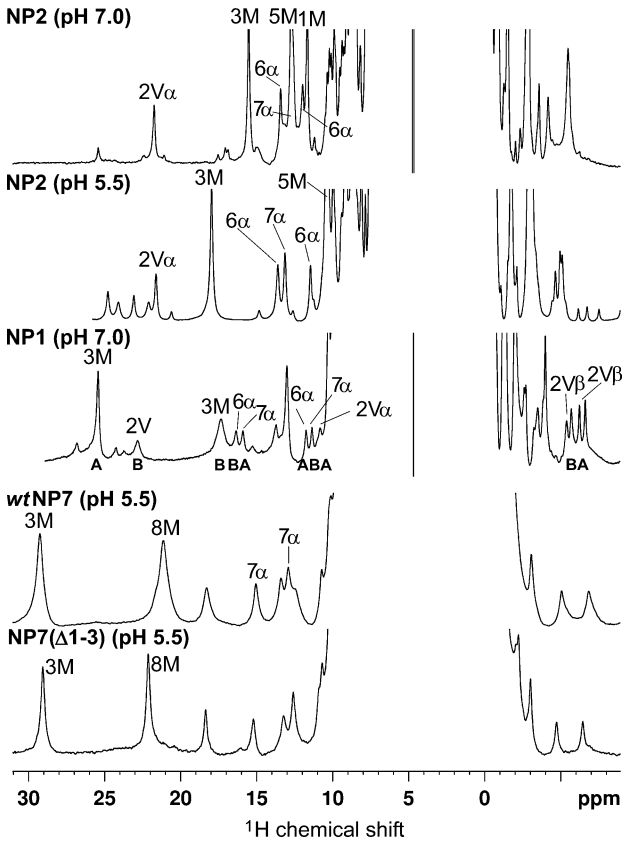

FIGURE 8: ^{1}H NMR spectra of the NP2−ImH complex at pH* 7.0 and 5.5, the NP1−ImH complex at pH* 7.0, and the *wt* NP7−ImH and NP7(Δ1−3)−ImH complexes, both at pH* 5.5. The proteins were dissolved in 30 mM NaD_2PO_4/NaOD (pH* 7.0) or 30 mM Na_2DPO_4/acetic acid-d_4 (pH* 5.5) at concentrations of 1−2 mM. ImD/acetic acid-d_4 solution in D_2O, titrated to either pH* 7.0 or 5.5, was added (final concentration of 20 mM) and spectra were recorded at 25 °C. The chemical shift assignments for the NP2−ImH and NP1−ImH complexes at pH* 7.0 are from previous literature (*23*, *24*) (1M, 3M, 5M, and 8M for heme methyl hydrogens; 2Vα and 2V*β* for heme vinyl $C^{\alpha}H$ and $C^{\beta}H_2$, respectively; 6α and 7α for the propionate $C^{\alpha}H_2$; numbering corresponds to the pyrrole ring *β*-carbons according to Scheme 4. **A** and **B** designate the two different heme orientations that have been assigned for NP1−ImH).

for any of the nitrophorin−ImH complexes (*23*, *24*, *27*). Until now, it has not been possible to obtain the assignment of the resonances by COSY and NOESY techniques, mostly due to the very short spin−spin relaxation times, T_2, that result in large linewidths, as well as the loss of magnetization before it can be acquired. Unusually severe line broadening also appeared in the high-spin spectra (data not shown) in comparison to those of NP1−4 (*22*). The decreased T_2 may be a result of charge ↔ charge interactions between individual NP7 molecules. As described above, it was previously reported that the surface opposite to the opening of the heme pocket, unlike the other nitrophorins, is highly positively charged (*38*). In addition, Figure 7B shows that the heme pocket entrance is, like the other nitrophorins, negatively charged, thus making NP7 a charge dipolar molecule. Interactions between NP7 molecules may lead to the transient formation of larger aggregates of various sizes which tumble more or less rapidly in the NMR sample solution and, thus, result in the decreased T_2 or spin−spin relaxation times. This hypothesis was supported by dynamic light scattering experiments in which *wt* NP7 (apparent hydrodynamic diameter of ∼40 Å) contained a large fraction of oligomers (apparent

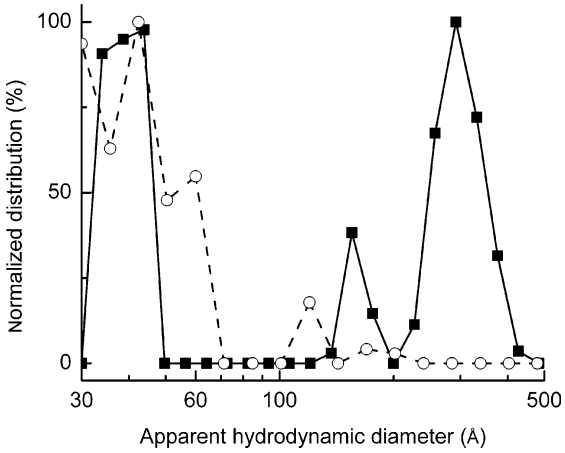

FIGURE 9: Dynamic light scattering of the NMR samples of (○) NP2−ImH (pH* 7.0) and (■) *wt* NP7−ImH (pH* 5.5) complexes reported in Figure 7. The normalized Rayleigh scattering was plotted versus the logarithm of the apparent hydrodynamic diameter.

hydrodynamic diameter of ∼250−400 Å), whereas NP2 was essentially free of oligomers (Figure 9).

However, integration of the two resonances at 29.3 and 21.2 ppm [29.7 and 22.1 ppm for NP7(Δ1−3)] in comparison to the resonances at 18.3, 15.1, 13.4, 13.0, and 12.5 ppm [18.3, 15.2, 13.2, and 12.6 ppm for NP7(Δ1−3)] suggest that they originate from heme methyl groups, whereas the latter, in comparison to ^{1}H NMR spectra of the other nitrophorin−ImH complexes, are likely $C^{\alpha}H_{1/2}$ of the vinyl and/or propionate groups (Scheme 4). Usually, the **A** orientation of the cofactor results in a large shift of the 3-methyl resonance to lower shielding, with that of the NP1−ImH and NP4−ImH complexes appearing at 25.1 and 25.7 ppm, respectively, at pH* 7.0 and 30 °C [compared to 17.0 and 16.4 ppm, respectively, for the **B** orientation (*23*); see Scheme 4]. The spectrum of the NP1−ImH complex at pH* 7.0, which exhibits an **A**:**B** ratio of ∼1.1:1, is included in Figure 8 (from ref *23*), where it can be seen that the 3-methyl resonance of isomer **A** is found at 25 ppm, while NP7 shows its lowest-shielding methyl resonance at ∼29 ppm. If this is the 3-methyl resonance, then the spectra obtained for the NP7−ImH complex are indicative of the **A** orientation, and the **B** orientation is not observed. Although the latter may be due to line broadening, in all other nitrophorins, the **A** orientation has always been found to be less abundant than **B** or similar in abundance to **B** (*22*−*24*, *27*). This is consistent with the spectra recorded for the high-spin NP7−H_2O species (data not shown) where chemical shifts, although being very broad, in comparison to those of NP1−4−H_2O complexes are indicative of the **A** orientation. Thus, NP7 appears to be the first nitrophorin that strongly favors the **A** heme orientation. Further assignments of the NMR signals will be presented elsewhere.

DISCUSSION

The reason why the "kissing bug", *R. prolixus*, pumps a set of seven nitrophorins into its victim's tissues during various life stages still remains a mystery. Moreover, during the six life stages of the insect that all feed on blood, different expression patterns of NP1−6 have been observed (*8*). NP7 has been missed in the isolation from salivary glands,

probably because of the use of isoelectric focusing chromatography over the pH range of 8.3−7.0, which is at closest ~1 pH unit below the pI of apo-NP7 [p*I* = 9.21 (Figure 1)]. NP7 was later found in a cDNA library derived from Vth instar nymphs; thus, it is not clear whether the protein is expressed in any of the other developmental stages. NP7 has the ability to inhibit prothrombinase activity through interaction with the prothrombinase activating L-α-phosphatidyl-L-serine (PS). The binding to PS is accomplished through charge ↔ charge interactions with the positively charged NP7 surface on the site opposite to the heme entrance site, a fact that contributes mainly to the high p*I* value (*39*, *45*). This function is unique among the *R. prolixus* nitrophorins. It may be noted, however, that NP2 can also inhibit the intrinsic Factor X activating complex, through binding with Factors IX and IX$_a$, which represents a third functionality of this protein besides NO delivery and histamine sequestration (*32*).

Nitrophorins are expressed in the endothelial cells of the salivary glands, and they are secreted into the extracellular space (*10*); thus, their as-expressed amino acid sequences are preceded by an N-terminal leader sequence (Figure 1). The software SignalP has been developed to predict the precise site of cleavage for the signal peptidase which was applied in the preceding study, and which proposed that the signal peptide should be cleaved three amino acids before the sites known for NP1−6 (*38*). The application of the novel, more accurate SignalP version 3.0 to the sequence of NP7 led to the NP7 cleavage site being the same as that previously published (Table 1). To rate the precision of the program for the prediction of native nitrophorin sequences, it was applied to NP1−4 amino acid sequences showing that an uncertainty remains. Thus, an NP7 construct, NP7(Δ1−3), lacking the ^{0}Met-Leu-Pro-Gly^{3} sequence was examined parallel to *wt* NP7 (Scheme 1).

Comparison of the results for both constructs clearly shows that NP7 needs its isoform-specific N-terminus for proper protein function. In particular, the higher thermostability of *wt* NP7 shows that the peptide interacts in a specific way with the rest of the polypeptide chain. Also, reduction potentials of *wt* NP7 were found to be within a reasonable range compared to those of the other nitrophorins (Table 3), whereas NP7(Δ1−3) has markedly more positive reduction potentials which may make it susceptible to reduction; as a consequence, NO release could not be accomplished. On the other hand, the very similar EPR and ^{1}H NMR spectra of the ImH complexes (Figure 8) suggest that the electronic structures of the heme iron, i.e., the heme orientation, the ImH plane orientation, and the degree of macrocycle ruffling, are nearly identical. Also, a mixed heme orientation could not be seen, and comparison with the NMR data from NP1−4 suggests a favored **A** orientation (Scheme 4) in contrast to the otherwise favored **B** orientation (*22*, *23*, *27*). A single heme orientation is also supported by the fact that no biphasic kinetics of the NO association and/or dissociation (Scheme 2) could be observed, which was recently ascribed to the presence of mixed **A**:**B** isomers with different rate constants (*44*). However, as described in the Results, in particular the differences in the histamine association constants, but not in the association constants of ImH (Table 2), indicate differences in the protein structure at the opening of the heme pocket.

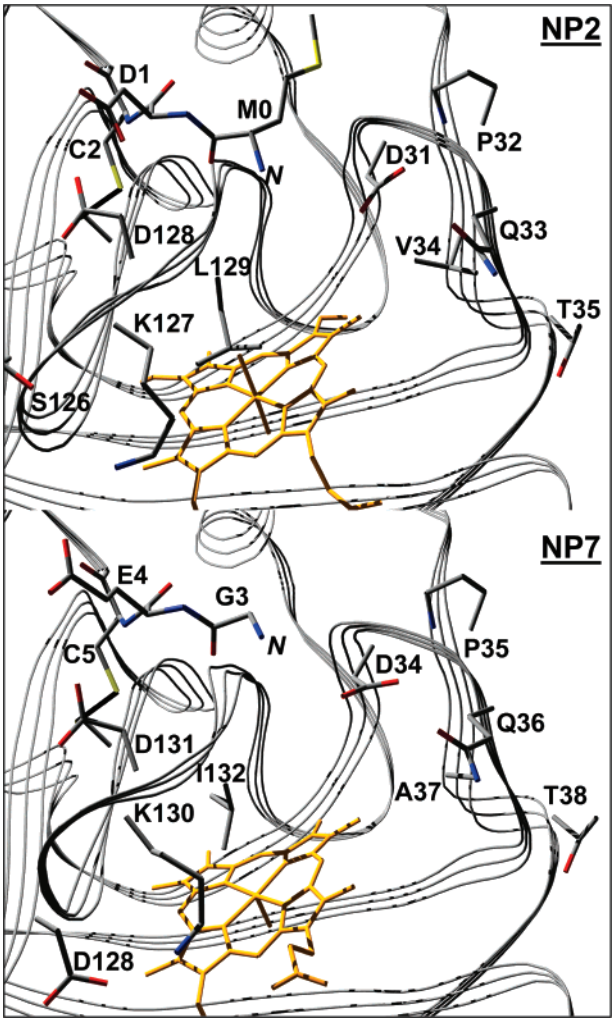

FIGURE 10: Comparison of the structural environment of the N-terminus of NP2 (PDB entry 1EUO) (top) with the homology model of NP7(G3−S182) (bottom). The residue numbering is according to Figure 1. Displayed are the heme cofactor (amber), the N-terminus (residues Met-0−Cys-2 of NP2 and Gly-3−Cys-5 of NP7), the A−B loop (residues Asp-31−Thr-35 of NP2 and Asp-34−Thr-38 of NP7), and the G−H loop (residues Gly-125−Leu-129 of NP2 and Asp-128−Ile-132 of NP7). Figures were prepared with DeepView version 3.7 and rendered with POV-Ray version 3.6 (http://www.povray.org).

Because Cys-5 in NP7 forms a disulfide bond with Cys-124, the N-terminus is highly constrained, and therefore, the relative position of the two residues, Leu-1 and Pro-2, of *wt* NP7 can be estimated to good approximation in the homology model of NP7(G3−S182) (Figure 7). As mentioned above, the N-terminus of NP4 was found to be involved in the closed loop structure of the A−B and G−H loops which were recognized to be of major importance for the NP4 histamine and NO binding kinetics (*30*). Therefore, a closer inspection of the NP7(G3−S182) model structure in comparison to the NP2 crystal structure was conducted (Figure 10). The structure in combination with the sequence alignment (Figure 1) shows that the A−B loops are almost identical, with the slight difference of Val-34 in NP2 being represented by Ala-37 in NP7 (see Figure 10). However, the much shorter G−H loop, which begins in all the other NPs with the motif $^{125/126}$Gly-(Gln/Pro/Ser)-Lys-Asp-Leu$^{129/130}$, is predicted to be represented by ^{128}Asp-Gly-Lys-Asp-Ile^{132} in NP7 (Figure 1). As a consequence, the formation of a salt

Scheme 5

$$NP{-}His{:}N^{\varepsilon}{-}Fe^{II}(pplX){-}NO + H^{+} \rightleftharpoons NP{-}His{:}N^{\varepsilon}H^{+} + Fe^{II}(pplX){-}NO$$

bridge between Asp-128 and Lys-130 [Asp:O^{γ} ↔ Lys:N^{ζ} = 2.9 Å (Figure 10)] is expected, which would increase the rigidity of the G−H loop. This may account for the different properties of NP7(Δ1−3) compared to those of NP1−4. On the other hand, the ^{1}Leu-Pro-Gly^{3} tail of *wt* NP7 is rather hydrophobic and will be repelled by the mostly polar A−B and G−H loops. However, the hydrophobic site of Ile-132 could interact with the ^{1}Leu-Pro-Gly^{3} peptide. In agreement with this hypothesis, the corresponding Leu-130 has been shown to have a major impact on the binding kinetics of NP4 (*30*).

Due to the recombinant expression of nitrophorins in *E. coli*, a Met-0 residue is added in the cases of NP1−3 that results from the translation of the start codon 5′-ATG-3′ (Scheme 1) (*44*). In contrast, NP4 was found to have the starting Met-0 cleaved off during expression in *E. coli* due to its unique Ala-1 (*34*). Mutation of Asp-1 of NP2 to Ala likewise resulted in the hydrolysis of Met-0 (Scheme 1) and resulted in a construct with a native length of the N-terminus. Studies of both constructs together with an NP2 construct that includes a four-residue addition,[8] $^{-3}$Gly-Ser-His-Met^{0}-NP2 (Scheme 1), revealed a difference in ^{1}H NMR chemical shifts for heme resonances and significantly slowed kinetics for ligand binding and the equilibration of the **A**:**B** ratio of the heme orientation (*44*). This was consistent with the crystal structure of the NP2(D1A) construct (PDB entry 2EU7), which shows a significantly more "closed loop" structure relative to the extended N-terminal constructs. However, the differences in reduction potentials and association constants between Met^{0}-NP2 and NP2(D1A) were rather small, suggesting that the Met-0 added to recombinant *wt* NP7 and NP7(Δ1−3) cannot account totally for the large differences between the two constructs reported in this study (Tables 2 and 3). Furthermore, *wt* NP7 shows significant thermodynamic changes compared to the truncated form, NP7(Δ1−3). This highlights the important role that the N-terminus plays in the native form of all the NPs.

Similar to NP7, a shift in the absorbance maximum of the Soret band to 395 nm upon reduction of the NO complex at pH 5.5 was observed and already mentioned for NP2^{II} and NP3^{II}, in contrast to NP1^{II} and NP4^{II} (*28*). The NP1^{II}−NO complex was noticed to be at least in part five-coordinate at low temperatures on the basis of EPR spectra at 4.2 K (*16*), indicating that labilization of the His:N^{ϵ}−Fe^{II} bond occurred due to the strong *trans* effect of the distal pocket NO ligand, as reported for a number of other heme proteins (*17*). However, the fact that the His:N^{ϵ}−Fe^{II} bond of nitrophorins is only broken at low pH suggests that the 100-fold increased [H^{+}], and thus imidazolium formation, contributes significantly to the appearance of the five-coordinate species according to Scheme 5.

In this context, the appearance of the five-coordinate species in the case of the NP7(Δ1−3)^{II}−NO complex at pH 7.5 rather than pH 5.5 is remarkable. As can be derived from Table 3, when the pH is increased from 5.5 to 7.5 the reduction potentials of all NP1−4−NO complexes decrease by −27 mV (NP1−NO) to −41 mV [NP2−NO; in the case of NP2(D1A)−NO even −68 mV]. Instead, in the case of the *wt* NP7−NO complex, a slight increase of +15 mV was measured. However, in the case of the NP7(Δ1−3)−NO complex, a marked increase of +71 mV occurred at pH 7.5, which indicates a major change in the heme binding pocket. Concomitantly, the reduction potential of the NP7(Δ1−3)−NO complex of +228 mV at pH 7.5 is unusually high.

While *R. prolixus* NP2, -3, and -7 and many other His-ligated heme proteins form a five-coordinate Fe^{II}−NO complex only at fairly low pH [e.g., cytochrome *c* at pH 2.0 (*66*)], there are a few examples of proteins that break the His:N−Fe^{II} bond even around neutral pH. Examples are the cytochrome *c*′ forms from various species (*67*−*69*). A very prominent but still little understood example of a mono-His heme protein, which loosens the His ligand upon NO binding, is the NO sensor soluble guanylate cyclase (sGC) (*70*, *71*). In this case, the NO-induced release of the proximal His triggers the activation of the catalytic center of sGC to form cGMP from GTP, which is used as a central second messenger in physiology. However, although this process is well-established, the exact molecular mechanism is still a matter of debate. Unlike NP7, sGC is a cytosolic protein and, consequently, exists in the Fe^{II} form, whereas the low reduction potential of the NP7−NO complex suggests that NP7 maintains the Fe^{III} form to keep its functionality. The +2 oxidation state of sGC is very sensitive to air oxidation, and this causes the problem of losing heme upon oxidation (*72*). We have been unable to find the exact reduction potential of sGC in the literature, but it can be assumed that it is rather low, since a very mild oxidant such as methylene blue [$E°$ = +11 mV at pH 7 (*73*)] readily oxidized the heme iron (*74*). Besides sGC, there are not many examples of proteins that release their proximal ligand upon NO binding. Human serum albumin (HSA) and the proximal His deletion mutant H93G of sperm whale Mb [Mb(H93G)] complexed to ImH have been used as models (*75*). The NP7(Δ1−3) mutant, however, provides a novel model system for studying the process that leads to five-coordination since it does not depend on low pH. Future studies along these lines are planned.

CONCLUSIONS

Our study shows that NP7 is a protein-based NO donor system as are NP1−4. However, NP7 has some remarkable functional differences which include (i) the largest difference in NO association constants between high and low pH, (ii) a small histamine affinity, suggesting that it will not contribute to histamine sequestration in vivo, (iii) large ^{1}H NMR chemical shifts for the Fe^{III} form of the protein, and (iv) strong favoring of the **A** orientation of the heme. Most of all, a unique N-terminal peptide, ^{1}Leu-Pro-Gly^{3}, is present, which contributes significantly to the protein fold stability. Moreover, the N-terminus is very important for maintenance of NP7 function.

ACKNOWLEDGMENT

We are grateful to Dr. Tatiana Kh. Shokhireva for helpful discussions, to Dr. Andrei V. Astashkin for recording the EPR spectra, and to Mr. David Roberts and Dr. Craig A.

[8] The NP2 form $^{-3}$Gly-Ser-His-Met^{0}-NP2 was obtained from the expression as an N-terminally His_6-tagged construct upon thrombin cleavage.

Aspinwall for help with the dynamic light scattering experiments (all from the Department of Chemistry, University of Arizona).

SUPPORTING INFORMATION AVAILABLE

Angle plot for low-spin ferrihemes (Figure S1). This material is available free of charge via the Internet at http://pubs.acs.org.

REFERENCES

1. Walker, F. A., and Montfort, W. R. (2001) in *Advances in Inorganic Chemistry* (Mauk, A. G., and Sykes, A. G., Eds.) Vol. 51, pp 295−358, Academic Press, San Diego.
2. Lehane, M. J. (2005) *The Biology of Blood-Sucking in Insects*, 2nd ed., Cambridge University Press, Cambridge, United Kingdom.
3. Zeledón, R., and Rabinovich, J. E. (1981) Chagas' disease: An ecological appraisal with special emphasis on its insect vectors, *Annu. Rev. Entomol. 26*, 101−133.
4. Kirchhoff, L. V. (1993) American trypanosomiasis (Chagas' disease): A tropical disease now in the United States, *N. Engl. J. Med. 329*, 639−644.
5. Wood, S. F. (1942) Observations on vectors of Chagas' disease in the United States. I. California, *Bull. Calif. Acad. Sci. 41*, 61−69.
6. Ribeiro, J. M. C., and Francischetti, I. M. B. (2003) Role of arthropode saliva in blood feeding: Sialome and post-sialome perspectives, *Annu. Rev. Entomol. 48*, 73−88.
7. Champagne, D. E., Nussenzveig, R. H., and Ribeiro, J. M. C. (1995) Purification, partial characterization, and cloning of nitric oxide-carrying heme proteins (nitrophorins) from salivary glands of the blood-sucking insect *Rhodnius prolixus*, *J. Biol. Chem. 270*, 8691−8695.
8. Moreira, M. F., Coelho, H. S. L., Zingali, R. B., Oliveira, P. L., and Masuda, H. (2003) Changes in salivary nitrophorin profile during the life cycle of the blood-sucking bug *Rhodnius prolixus*, *Insect Biochem. Mol. Biol. 33*, 23−28.
9. Ribeiro, J. M. C., and Nussenzveig, R. H. (1993) Nitric oxide synthase activity from a hematophagous insect salivary gland, *FEBS Lett. 330*, 165−168.
10. Nussenzveig, R. H., Bentley, D. L., and Ribeiro, J. M. C. (1995) Nitric oxide loading of the salivary nitric-oxide-carrying hemoproteins (nitrophorins) in the blood-sucking bug *Rhodnius prolixus*, *J. Exp. Biol. 198*, 1093−1098.
11. Yuda, M., Hirai, M., Miura, K., Matsumura, H., Ando, K., and Chinzei, Y. (1996) cDNA cloning, expression and characterization of nitric-oxide synthase from the salivary glands of the blood-sucking insect *Rhodnius prolixus*, *Eur. J. Biochem. 242*, 807−812.
12. Soares, A. C., Carvalho-Tavares, J., Gontijo, N. d. F., dos Santos, V. C., Teixeira, M. M., and Pereira, M. H. (2006) Salivation pattern of *Rhodnius prolixus* (Reduviidae; Triatominae) in mouse skin, *J. Insect Physiol. 52*, 468−472.
13. Ribeiro, J. M. C., Hazzard, J. M., Nussenzveig, R. H., Champagne, D. E., and Walker, F. A. (1993) Reversible binding of nitric oxide by a salivary heme protein from a bloodsucking insect, *Science 260*, 539−541.
14. Hoshino, M., Maeda, M., Konishi, R., Seki, H., and Ford, P. C. (1996) Studies on the reaction mechanism for reductive nitrosylation for ferrihemoproteins in buffer solutions, *J. Am. Chem. Soc. 118*, 5702−5707.
15. Shokhireva, T. Kh., Berry, R. E., Uno, E., Balfour, C. A., Zhang, H., and Walker, F. A. (2003) Electrochemical and NMR spectroscopic studies of distal pocket mutants of nitrophorin 2: Stability, structure, and dynamics of axial ligand complexes, *Proc. Natl. Acad. Sci. U.S.A. 100*, 3778−3783.
16. Ding, X. D., Weichsel, A., Andersen, J. F., Shokhireva, T. Kh., Balfour, C., Pierik, A. J., Averill, B. A., Montfort, W. R., and Walker, F. A. (1999) Nitric oxide binding to the ferri- and ferroheme states of nitrophorin 1, a reversible NO-binding heme protein from the saliva of the blood-sucking insect, *Rhodnius prolixus*, *J. Am. Chem. Soc. 121*, 128−138.
17. Traylor, T. G., and Sharma, V. S. (1992) Why NO? *Biochemistry 31*, 2847−2849.
18. Watt, A. P., and Ennis, M. (2004) Characterization of histamine release by mast cells, basophils, and monocytes, in *Histamine: Biology and Medical Aspects* (Falus, A., Grosman, N., and Darvas, Z., Eds.) pp 99−111, SpringMed Publishing Ltd., Budapest.
19. Ribeiro, J. M. C., and Walker, F. A. (1994) High affinity histamine-binding and antihistaminic activity of the salivary nitric oxide-carrying heme protein (nitrophorin) of *Rhodnius prolixus*, *J. Exp. Med. 180*, 2251−2257.
20. Maes, E. M., Walker, F. A., Montfort, W. R., and Czernuszewicz, R. S. (2001) Resonance Raman spectroscopic study of nitrophorin 1, a nitric oxide-binding heme protein from *Rhodnius prolixus*, and its nitrosyl and cyano adducts, *J. Am. Chem. Soc. 123*, 1164−1172.
21. Berry, R. E., Ding, X. D., Shokhireva, T. Kh., Weichsel, A., Montfort, W. R., and Walker, F. A. (2004) Axial ligand complexes of the *Rhodnius nitrophorins*: Reduction potentials, binding constants, EPR spectra, and structures of the 4-iodopyrazole and imidazole complexes of NP4, *J. Biol. Inorg. Chem. 9*, 135−144.
22. Shokhireva, T. Kh., Smith, K. M., Berry, R. E., Shokhirev, N. V., Balfour, C. A., Zhang, H., and Walker, F. A. (2007) Assignment of the ferriheme resonances of the high-spin forms of nitrophorins 1 and 4 by ^{1}H NMR spectroscopy: Comparison to structural data obtained from X-ray crystallography, *Inorg. Chem. 46*, 170−178.
23. Shokhireva, T. Kh., Weichsel, A., Smith, K. M., Berry, R. E., Shokhirev, N. V., Balfour, C. A., Zhang, H., Montfort, W. R., and Walker, F. A. (2007) Assignment of the ferriheme resonances of the low-spin complexes of nitrophorins 1 and 4 by ^{1}H and ^{13}C NMR spectroscopy: Comparison to structural data obtained from X-ray crystallography, *Inorg. Chem. 46*, 2041−2056.
24. Shokhireva, T. Kh., Shokhirev, N. V., and Walker, F. A. (2003) Assignment of heme resonances and determination of the electronic structures of high- and low-spin nitrophorin 2 by ^{1}H and ^{13}C NMR spectroscopy: An explanation of the order of heme methyl resonances in high-spin ferriheme proteins, *Biochemistry 42*, 679−693.
25. Wegner, P., Benda, R., Schünemann, V., Trautwein, A. X., Berry, R. E., Balfour, C. A., Wert, D., and Walker, F. A. (2002) Insect bites on a molecular basis. How does the blood-sucking bug *Rhodnius prolixus* get its meal? The ferriheme proteins nitrophorin 2 and 4 studied by Mössbauer spectroscopy, *Hyperfine Interact. C5*, 253−256.
26. Astashkin, A. V., Raitsimring, A. M., and Walker, F. A. (1999) Two- and four-pulse ESEEM studies of the heme binding center of a low-spin ferriheme protein: The importance of a multifrequency approach, *Chem. Phys. Lett. 306*, 9−17.
27. Shokhireva, T. Kh., Berry, R. E., Zhang, H., Shokhirev, N. V., and Walker, F. A. (2007) Assignment of ferriheme resonances for high- and low-spin forms of nitrophorin 3 by ^{1}H and ^{13}C NMR spectroscopy and comparison to nitrophorin 2: Heme pocket structural similarities and differences, *Inorg. Chim. Acta* (in press).
28. Andersen, J. F., Ding, X. D., Balfour, C., Shokhireva, T. Kh., Champagne, D. E., Walker, F. A., and Montfort, W. R. (2000) Kinetics and equilibria in ligand binding by nitrophorins 1−4: Evidence for stabilization of a nitric oxide-ferriheme complex through a ligand-induced conformational trap, *Biochemistry 39*, 10118−10131.
29. Andersen, J. F., Champagne, D. E., Weichsel, A., Ribeiro, J. M. C., Balfour, C. A., Dress, V., and Montfort, W. R. (1997) Nitric oxide binding and crystallization of recombinant nitrophorin I, a nitric oxide transport protein from the blood-sucking bug *Rhodnius prolixus*, *Biochemistry 36*, 4423−4428.
30. Maes, E. M., Weichsel, A., Andersen, J. F., Shepley, D., and Montfort, W. R. (2004) Role of binding site loops in controlling nitric oxide release: Structure and kinetics of mutant forms of nitrophorin 4, *Biochemistry 43*, 6679−6690.
31. Weichsel, A., Andersen, J. F., Champagne, D. E., Walker, F. A., and Montfort, W. R. (1998) Crystal structures of a nitric oxide transport protein from a blood-sucking insect, *Nat. Struct. Biol. 5*, 304−309.
32. Andersen, J. F., and Montfort, W. R. (2000) The crystal structure of nitrophorin 2. A trifunctional antihemostatic protein from the saliva of *Rhodnius prolixus*, *J. Biol. Chem. 275*, 30496−30503.
33. Andersen, J. F., Weichsel, A., Balfour, C. A., Champagne, D. E., and Montfort, W. R. (1998) The crystal structure of nitrophorin 4 at 1.5 Å resolution: Transport of nitric oxide by a lipocalin-based heme protein, *Structure 6*, 1315−1327.

34. Weichsel, A., Andersen, J. F., Roberts, S. A., and Montfort, W. R. (2000) Nitric oxide binding to nitrophorin 4 induces complete distal pocket burial, *Nat. Struct. Biol. 7*, 551−554.
35. Roberts, S. A., Weichsel, A., Qiu, Y., Shelnutt, J. A., Walker, F. A., and Montfort, W. R. (2001) Ligand-induced heme ruffling and bent NO geometry in ultra-high-resolution structures of nitrophorin 4, *Biochemistry 40*, 11327−11337.
36. Montfort, W. R., Weichsel, A., and Andersen, J. F. (2000) Nitrophorins and related antihemostatic lipocalins from *Rhodnius prolixus* and other blood-sucking arthropods, *Biochim. Biophys. Acta 1482*, 110−118.
37. Ribeiro, J. M. C., Andersen, J. F., Silva-Neto, M. A. C., Pham, V. M., Garfield, M. K., and Valenzuela, J. G. (2004) Exploring the sialome of the blood-sucking bug *Rhodnius prolixus*, *Insect Biochem. Mol. Biol. 34*, 61−79.
38. Andersen, J. F., Gudderra, N. P., Francischetti, I. M. B., Valenzuela, J. G., and Ribeiro, J. M. C. (2004) Recognition of anionic phospholipid membranes by an antihemostatic protein from a blood-feeding insect, *Biochemistry 43*, 6987−6994.
39. Andersen, J. F., Gudderra, N. P., Francischetti, I. M. B., and Ribeiro, J. M. C. (2005) The role of salivary lipocalins in blood feeding by *Rhodnius prolixus*, *Arch. Insect Biochem. Physiol. 58*, 97−105.
40. Callahan, M. K., Williamson, P., and Schlegel, R. A. (2000) Surface expression of phosphatidylserine on macrophages is required for phagocytosis of apoptotic thymocytes, *Cell Death Differ. 7*, 645−653.
41. Hirt, U. A., and Leist, M. (2003) Rapid, noninflammatory and PS-dependent phagocytic clearance of necrotic cells, *Cell Death Differ. 10*, 1156−1164.
42. Ignarro, L. J. (1990) Biosynthesis and metabolism of endothelium-derived nitric oxide, *Annu. Rev. Pharmacol. Toxicol. 30*, 535−560.
43. Weichsel, A., Maes, E. M., Andersen, J. F., Valenzuela, J. G., Shokhireva, T. Kh., Walker, F. A., and Montfort, W. R. (2005) Heme-assisted S-nitrosation of a proximal thiolate in a nitric oxide transport protein, *Proc. Natl. Acad. Sci. U.S.A. 102*, 594−599.
44. Berry, R. E., Shokhireva, T. Kh., Filippov, I., Shokhirev, M. N., Zhang, H., and Walker, F. A. (2007) The effect of the N-terminus on heme cavity structure, ligand equilibrium and rate constants and reduction potentials of nitrophorin 2 from *Rhodnius prolixus*, *Biochemistry 46*, 6830−6843.
45. Knipp, M., Zhang, H., Berry, R. E., and Walker, F. A. (2007) Overexpression in *Escherichia coli* and functional reconstitution of the liposome binding ferriheme protein nitrophorin 7 from the blood sucking bug *Rhodnius prolixus*, *Protein Expression Purif. 54*, 183−191.
46. Zhang, X., Cardossa, L., Broderick, M., Fein, H., and Davies, I. R. (2000) Novel calibration method for nitric oxide microsensors by stoichiometric generation of nitric oxide from SNAP, *Electroanalysis 12*, 425−428.
47. Edgar, R. C. (2004) MUSCLE: Multiple sequence alignment with high accuracy and high throughput, *Nucleic Acids Res. 32*, 1792−1797.
48. Schwede, T., Kopp, J., Guex, N., and Peitsch, M. C. (2003) SWISS-MODEL: An automated protein homology-modeling server, *Nucleic Acids Res. 31*, 3381−3385.
49. Peitsch, M. C. (1995) Protein modeling by E-mail, *Bio/Technology 13*, 658−660.
50. Guex, N., and Peitsch, M. C. (1997) SWISS-MODEL and the Swiss-PdbViewer: An environment for comparative protein modeling, *Electrophoresis 18*, 2714−2723.
51. Hooft, R. W., Vriend, G., Sander, C., and Abola, E. E. (1996) Errors in protein structures, *Nature 381*, 272.
52. Laskowski, R. A., MacArthur, M. W., Moss, D., and Thornton, J. M. (1993) PROCHECK: A program to check the stereochemical quality of protein structures, *J. Appl. Crystallogr. 26*, 283−291.
53. Ribeiro, J. M. C., Schneider, M., and Guimarães, J. A. (1995) Purification and characterization of prolixin S (nitrophorin 2), the salivary anticoagulant of the blood-sucking bug *Rhodnius prolixus*, *Biochem. J. 308*, 243−249.
54. Nielsen, H., Engelbrecht, J., Brunak, S., and von Heijne, G. (1997) Identification of prokaryotic and eukaryotic signal peptides and prediction of their cleavage sites, *Protein Eng. 10*, 1−6.
55. Bendtsen, J. D., Nielsen, H., von Heijne, G., and Brunak, S. (2004) Improved prediction of signal peptides: SignalP 3.0, *J. Mol. Biol. 340*, 783−795.
56. Nielsen, H., and Krogh, A. (1998) in *Proceedings of the Sixth International Conference on Intelligent Systems for Molecular Biology (ISMB 6)*, pp 122−130, AAAI Press, Menlo Park, CA.
57. Jochem, J., and Żwirska-Korczala, K. W. (2004) Histamine in the cardiovascular system, in *Histamine: Biology and Medical Aspects* (Falus, A., Grosman, N., and Darvas, Z., Eds.) pp 303−316, SpringMed Publishing Ltd., Budapest.
58. Yoshimura, T. (1983) Q-Band electron paramagnetic resonance study of nitrosylprotoheme dimethyl ester complexes with N-, O-, and S-donor ligand as model systems for nitrosylhemoproteins, *J. Inorg. Biochem. 18*, 263−277.
59. Brunori, M., Falcioni, G., and Rotilio, G. (1974) Kinetic properties and electron paramagnetic resonance spectra of the nitric oxide derivative of hemoglobin components of trout (*Salmo irideus*), *Proc. Natl. Acad. Sci. U.S.A. 71*, 2470−2472.
60. Cheng, L., and Richter-Addo, G. B. (2000) Binding and activation of nitric oxide by metalloporphyrins and heme, in *The Porphyrin Handbook* (Kadish, K. M., Smith, K. M., and Guilard, R., Eds.) Vol. 4, pp 219−291, Academic Press, San Diego.
61. Wittung-Stafshede, P., Mamström, B. G., Winkler, J. R., and Gray, H. B. (1998) Folding of deoxymyglobin triggered by electron transfer, *J. Phys. Chem. A 102*, 5599−5601.
62. Wittung-Stafshede, P. (1999) Effect of redox state on unfolding energetics of heme proteins, *Biochim. Biophys. Acta 1432*, 401−405.
63. Yatsunyk, L. A., Carducci, M. D., and Walker, F. A. (2003) Low-spin ferriheme models of the cytochromes: Correlation of molecular structure with EPR spectral type, *J. Am. Chem. Soc. 125*, 15986−16005.
64. La Mar, G. N., Burns, P. D., Jackson, J. T., Smith, K. M., Langry, K. C., and Strittmatter, P. (1981) Proton magnetic resonance determination of the relative heme orientations in disordered native and reconstituted ferricytochrome b_5. Assignment of heme resonances by deuterium labeling, *J. Biol. Chem. 256*, 6075−6079.
65. Walker, F. A., Emrick, D., Rivera, J. E., Hanquet, B. J., and Buttlaire, D. H. (1988) Effect of heme orientation on the reduction potential of cytochrome b_5, *J. Am. Chem. Soc. 110*, 6234−6240.
66. Yoshimura, T., and Suzuki, S. (1988) The pH dependence of the stereochemistry around the heme group in NO-cytochrome *c* (horse heart), *Inorg. Chim. Acta 152*, 241−249.
67. Suzuki, S., Yoshimura, T., Nakahara, A., Iwasaki, H., Shidara, S., and Matsubara, T. (1987) Electronic and magnetic circular dichroism spectra of pentacoordinate nitrosulhemes in cytochromes *c′* from nonphotosynthetic bacteria and their model complexes, *Inorg. Chem. 26*, 1006−1008.
68. Iwasaki, H., Yoshimura, T., Suzuki, S., and Shidara, S. (1991) Spectral properties of *Achromobacter xylosoxidans* cytochrome *c′* and their NO complexes, *Biochim. Biophys. Acta 1058*, 79−82.
69. Yoshimura, T., Fujii, S., Kamada, H., Yamaguchi, K., Suzuki, S., Shidara, S., and Takakuwa, S. (1996) Spectroscopic characterization of nitrosylheme in nitric oxide complexes of ferric and ferrous cytochrome *c′* from photosynthetic bacteria, *Biochim. Biophys. Acta 1292*, 39−46.
70. Sharma, V. S., and Madge, D. (1999) Activation of soluble guanylate cyclase by carbon monoxide and nitric oxide: A mechanistic model, *Methods 19*, 494−505.
71. Hobbs, A. J. (1997) Soluble guanylate cyclase: The forgotten sibling, *Trends Pharmacol. Sci. 18*, 484−491.
72. Burstyn, J. N., Yu, A. E., Dierks, E. A., Hawkins, B. K., and Dawson, J. H. (1995) Studies of the heme coordination and ligand binding properties of soluble guanylate cyclase (sGC): Characterization of Fe(II)sGC and Fe(II)sGC(CO) by electronic absorption and magnetic circular dichroism spectroscopy and failure of CO to activate the enzyme, *Biochemistry 34*, 5896−5903.
73. Fasman, C. D. (1976) *Handbook of Biochemistry and Molecular Biology*, 3rd ed., CRC Press, Boca Raton, FL.
74. Dierks, E. A., and Burstyn, J. N. (1998) The deactivation of soluble guanylyl cyclase by redox-active agents, *Arch. Biochem. Biophys. 351*, 1−7.
75. Kharitonov, V. G., Sharma, V. S., Magde, D., and Koesling, D. (1997) Kinetics of nitric oxide dissociation from five- and six-coordinate nitrosyl hemes and heme proteins, including soluble guanylate cyclase, *Biochemistry 36*, 6814−6818.

BI7014986